



CAPTURE OF TRANS-NEPTUNIAN PLANETESIMALS IN THE MAIN ASTEROID BELT

DAVID VOKROUHLICKÝ¹, WILLIAM F. BOTTKE², AND DAVID NESVORNÝ²

¹Institute of Astronomy, Charles University, V Holešovičkách 2, CZ-18000 Prague 8, Czech Republic; vokrouhl@cesnet.cz

²Department of Space Studies, Southwest Research Institute, 1050 Walnut Street, Suite 300, Boulder, CO 80302;
bottke@boulder.swri.edu, davidn@boulder.swri.edu

Received 2016 February 9; accepted 2016 April 21; published 2016 July 26

ABSTRACT

The orbital evolution of the giant planets after nebular gas was eliminated from the Solar System but before the planets reached their final configuration was driven by interactions with a vast sea of leftover planetesimals. Several variants of planetary migration with this kind of system architecture have been proposed. Here, we focus on a highly successful case, which assumes that there were once five planets in the outer Solar System in a stable configuration: Jupiter, Saturn, Uranus, Neptune, and a Neptune-like body. Beyond these planets existed a primordial disk containing thousands of Pluto-sized bodies, ~ 50 million $D > 100$ km bodies, and a multitude of smaller bodies. This system eventually went through a dynamical instability that scattered the planetesimals and allowed the planets to encounter one another. The extra Neptune-like body was ejected via a Jupiter encounter, but not before it helped to populate stable niches with disk planetesimals across the Solar System. Here, we investigate how interactions between the fifth giant planet, Jupiter, and disk planetesimals helped to capture disk planetesimals into both the asteroid belt and first-order mean-motion resonances with Jupiter. Using numerical simulations, we find that our model produces the right proportion of P- and D-type asteroids in the inner, central, and outer main belt, while also populating the Hilda and Thule regions in Jupiter's $3/2$ and $4/3$ resonances. Moreover, the largest observed P/D types in each sub-population are an excellent fit to our captured population results (within uncertainties). The model produces a factor of ~ 10 overabundance of diameter $D > 10$ km P/D types in the main belt, but this mismatch can likely be explained by various removal mechanisms (e.g., collision evolution over 4 Gyr, dynamical losses via Yarkovsky thermal forces over 4 Gyr, thermal destruction of the planetesimals en route to the inner solar system). Overall, our instability model provides a more satisfying match to constraints than that of Levison et al., and it provides us with strong supporting evidence that the five giant planet instability model is reasonable. Our results lead us to predict that D-type asteroids found in the near-Earth object population on low delta- V orbits with Earth are the surviving relics from the same source population that now make up the Kuiper Belt, the irregular satellites, and the Jupiter Trojans. The singular Tagish Lake meteorite, a primitive sample unlike other carbonaceous chondrite meteorites, is likely a fragment from a D-type asteroid implanted into the inner main belt. This would effectively make it the first known hand sample with the same composition as Kuiper Belt objects.

Key words: minor planets, asteroids: general – planets and satellites: dynamical evolution and stability

1. INTRODUCTION

When giant planets are forming, they can interact both with each other and with the massive gaseous nebula surrounding them. Observations of exoplanetary systems and numerical simulations (e.g., Masset & Snellgrove 2001; Morbidelli & Crida 2007, Pierens & Raymond 2011) suggest that this behavior places them in compact and resonant configurations. Curiously, while we do not expect our giant planets to be exceptions to this rule, their observed orbits are neither resonant nor in a compact configuration. This has led researchers to argue that the orbits of our giant planets must have undergone substantial dynamical evolution after the solar nebular gas disappeared from our Solar system. This so-called late migration phase, driven by angular momentum exchange between the planets and residual planetesimals in a vast disk, presumably allowed our giant planets to move from their original compact and resonant configuration to their current orbits. The putative planetesimal disk was likely located beyond the orbit of Neptune, which is a much safer locale than between the giant planets. It has been estimated that such a disk might have had a total mass of several tens of Earth masses (e.g., Tsiganis et al. 2005; Nesvorný & Morbidelli 2012).

The nature of the Kuiper Belt population, with numerous objects in resonance with Neptune, has independently led to a consensus that the giant planets had to undergo late migration. A detailed description how this process took place, however, is still being debated. For example, initial calculations predicted that the giant planets experienced smooth and slow migration (e.g., Malhotra 1995; Hahn & Malhotra 1999). These models, while providing useful insights, have not yet been able to reproduce the orbits of the small-body populations in the outer solar system. Instead, it has been recognized that a short period of instability, when the giant planets interacted with one another during close encounters, may be needed to match all of the constraints. Emerging from the original model of Thommes et al. (1999), the most quoted variant of a dynamical instability leading to late migration has been the “Nice model” (Tsiganis et al. 2005). Here, the instability was triggered by a combination of several factors. Neptune, initially parked close to the planetesimal disk, slowly perturbed disk objects into the zone of the gas giants. Planetary interactions eventually allowed the bodies to reach Jupiter, which promptly threw them out of the Solar System. This led Jupiter to migrate slowly inward, while Saturn, Uranus, and Neptune migrated slowly outward. Eventually, Jupiter and Saturn crossed their mutual $2/1$ mean-motion resonance, which destabilized Uranus and

Neptune and sent them into the disk. The resulting interactions allowed all of the giant planets to reach their observed orbits, with the byproducts being the Trojan asteroids, irregular satellites, Kuiper Belt, and scattered disk populations.

While compelling in many aspects, the original variant of the Nice model has certain drawbacks. The assumed starting orbits of the giant planets were chosen in an ad hoc fashion; they were not based on models of their formation processes or how they would undergo early dynamical evolution in the solar nebula (see, however, Morbidelli et al. 2007 and Levison et al. 2011 as intended pathways to fix this problem). In addition, given Jupiter's mass dominance, encounters between Jupiter and planets often lead to the planet being flung from the Solar System. This meant that the most successful runs of the original Nice model were frequently those where Saturn, Uranus, and Neptune avoided Jupiter encounters. Unfortunately, the absence of such encounters leads to new problems, in that these trials fail to preserve the orbital nature of the terrestrial planets and asteroid belt.

A clever solution was offered by Brasser et al. (2009) and Morbidelli et al. (2010). They showed that having Jupiter “jump” to new orbits as a consequence of giant planet encounters could save the terrestrial planets and asteroid belt. Moreover, the magnitudes of the jumps were naturally produced by having Jupiter encounter a Uranus/Neptune-like giant planet. These encounters also allowed Jupiter to obtain its observed population of irregular satellites (e.g., Jewitt & Haghighipour 2007; Nicholson et al. 2008), with scattered bodies from the planetesimal disk captured during three-body reactions between Jupiter, a Uranus/Neptune-like giant planet, and the comet (e.g., Nesvorný et al. 2007, 2013). This takes us back to square one, however, with Jupiter being likely to eject the giant planet that dares to enter its realm.

A possible resolution to this conundrum has been presented by Nesvorný (2011) and Batygin et al. (2012). They postulated that our Solar System originally contained three ice giants rather than the two observed. This is easily allowed by planet formation models. The additional giant was assumed to reside between Jupiter–Saturn and Uranus–Neptune. This ill-fated fifth planet is sent by Saturn to the Jupiter orbital zone during the dynamical instability, where it was subsequently scattered away. Before it left, though, it provided Jupiter with its needed jumps. Encounters with the fifth planet also provide large semimajor axis kicks to Neptune. It can be shown that this scenario can explain certain orbital features in the trans-Neptunian population (e.g., Nesvorný 2015b; Nesvorný & Vokrouhlický 2016).

Note that in this evolutionary variant, the giant planets start in a tight but stable resonant configuration, as suggested by planet formation models (Nesvorný 2011; Batygin et al. 2012). This removes the criticism of the giant planet ad hoc starting orbits in the original Nice model. Up to now, the most successful models have had Jupiter and Saturn start in their mutual 3/2 resonance rather than their 2/1 resonance (e.g., Brasser et al. 2009). The dynamical instability then occurs when Jupiter and Saturn leave their mutual resonance.

Nesvorný & Morbidelli (2012, NM12) have studied the five-giant-planet model in considerable detail. Their successful simulations have motivated further studies, with the goal of critically testing whether these new frameworks can match additional Solar System constraints (e.g., orbits of terrestrial planets, orbits of the asteroid belt, etc.). For example, using the

NM12 five-planet scenario, (i) Nesvorný et al. (2013) examined whether the capture of disk planetesimals could reproduce the Jupiter Trojan swarms; (ii) Nesvorný et al. (2014a) explored how planetesimals could have been captured by Jupiter and other giant planets onto orbits similar to irregular satellites; (iii) Deienno et al. (2014), Nesvorný et al. (2014b), and Cloutier et al. (2015) studied the stability and possible excitation of orbits of regular satellites of Jupiter and Saturn; (iv) Nesvorný (2015a, 2015b) and Nesvorný & Vokrouhlický (2016) studied the effect of this model on the orbital architecture of trans-Neptunian objects; (v) Roig & Nesvorný (2015) analyzed how this scenario affected the orbits of main belt asteroids; and (vi) Vokrouhlický & Nesvorný (2015) and Brasser & Lee (2015) investigated subtle dynamical effects that could have tipped over the spin axes of Jupiter and Saturn during the pre- and post-instability migration phases. All of these works indicate that NM12 is a fully viable scenario for the giant planet orbital evolution. Despite their successes, however, we cannot yet prove that the giant planets *must* have evolved as described by NM12. Therefore, here, we continue the quest by examining yet another implication of the NM12 models.

As discussed above, the small-body populations in the Solar System provide a diagnostic of what the orbits of giant planets have been doing in the past. The nearest, and thus the best characterized, reservoir that we can use are the main-belt asteroids. Indeed, as reviewed by Morbidelli et al. (2015), the main belt reveals traces of the excitation process, or processes,³ both in the orbital and in the taxonomic distributions versus semimajor axis. These perturbations have been studied by Roig & Nesvorný (2015) within the NM12 framework.

Here, we investigate another possible tracer of ancient dynamical excitation events found in the asteroid belt. The main belt has numerous C-complex asteroids, bodies with spectra similar to the known carbonaceous chondrites. A particularly interesting group associated with these asteroids, with low albedos and steep featureless spectra, are the P- and D-type asteroids (e.g., DeMeo et al. 2015). These bodies are modestly rare across the main belt, but they are common in the populations located at larger semimajor axes, such as the Hilda asteroids, Jupiter Trojan asteroids, Jupiter-family comets (JFCs), and irregular satellites (Jewitt & Haghighipour 2007; Nicholson et al. 2008; DeMeo et al. 2015). Moreover, applications of the Nice model suggest that these latter populations were created from objects scattered out of the trans-Neptunian planetesimal disk. If true, then perhaps the P/D types in the main belt were captured in a similar manner.

This idea was first suggested and then tested by Levison et al. (2009) using the original Nice model framework. They could indeed capture in their simulations many P/D types in the main belt on orbits consistent with those observed. However, their model had certain limitations that warrant a closer examination using the NM12 scenario.

For instance, Levison et al. (2009) found that the implantation probability of P/D-type asteroids into the main belt and Hilda population was rather large, such that they captured many more bodies of a given size than those observed. Their way to reconcile this problem was to assume that many of the captured bodies were weak enough that they were collisionally destroyed over billions of years by other main belt asteroids. This scenario could be reasonable, and their modeling of the

³ It is also possible that the main belt has been affected by multiple dynamical excitation events.

process did produce successful results, but at the cost of arguing that P/D types disrupt very easily. While the jury is still out on this precise question, recent studies indicate that C-complex asteroids, many which are low-density, porous bodies, are stronger from a collisional disruption perspective than previously suspected (Jutzi et al. 2015). This may present problems for the Levison et al. (2009) scenario.

A second issue is that the simulations of Levison et al. (2009) indicated that captured planetesimals could not reach semimajor axes $a < 2.68$ au (between the J3/1 and J5/2 mean-motion resonances with Jupiter). This is arguably a reasonable result, with the vast majority of P/D types in the main belt conforming to such orbits. More recent observations reported by DeMeo et al. (2014, 2015, see also DeMeo & Carry 2014), however, confirm a distinct tail of D-type objects extending into the inner main belt ($a < 2.5$ au, the location of the J3/1 resonance).⁴ This suggests that the Levison et al. (2009) simulations are missing some key part of the dynamical problem and raises intriguing questions concerning the nature of the implantation process.

We hypothesize that the jumping-Jupiter, five-planet instability variant defined by NM12 might resolve some of the problems discussed above. The new model components here would be that the ice giant ejected by Jupiter may dynamically affect the main belt in some manner. This issue has yet to be examined by any paper. For instance, gravitational interactions between this ice giant and planetesimals ejected from the trans-Neptunian disk could potentially place P/D-type bodies into the inner main belt. It should also modify the capture efficiency of P/D types into the main belt and Hilda asteroid regions. Ideally, this could provide a rationale to lower the amount of collisional destruction needed in the Levison et al. (2009) scenario to match observational constraints.

Here, we model this possibility using the NM12 framework. Specifically, we use selected NM12 simulations in order to analyze how planetesimals from the trans-Neptunian disk were captured into the main belt. Specific sub-populations, such as those objects residing in first-order, mean-motion resonances with Jupiter will also be carefully examined. In Section 2, we describe some details of our numerical simulations, while in Section 3, we analyze their results and compare them with available constraints. Finally, in Sections 4 and 5, we provide further discussion and conclusions.

2. CAPTURE SIMULATIONS OF P/D-TYPE BODIES

Our simulations were designed to be identical to those described in Nesvorný et al. (2013), who studied the capture of P/D-type bodies into the L4 and L5 Jupiter Trojan asteroid populations. In fact, we partly made use of their results, but greatly expanded upon them in order to be able to describe processes with much smaller capture probabilities. This extension is required because the number and sizes of P/D-type asteroids in the inner main belt are fairly small compared to the observed Trojan population. In quantitative terms, there are four confirmed D-type asteroids in the inner main belt

⁴ In fact, it has long been suggested that objects with featureless and steep spectra exist across a larger portion of the main belt, but their exact nature and relation to their more canonical twins in the Hilda and Trojans regions was discussed (see, e.g., Lagerkvist et al. 1993; Fitzsimmons et al. 1994; Carvano et al. 2003). This was also because these earlier works lacked substantiation by the absence of spectral information extending to the near-infrared part of the spectrum. This is now becoming commonly available.

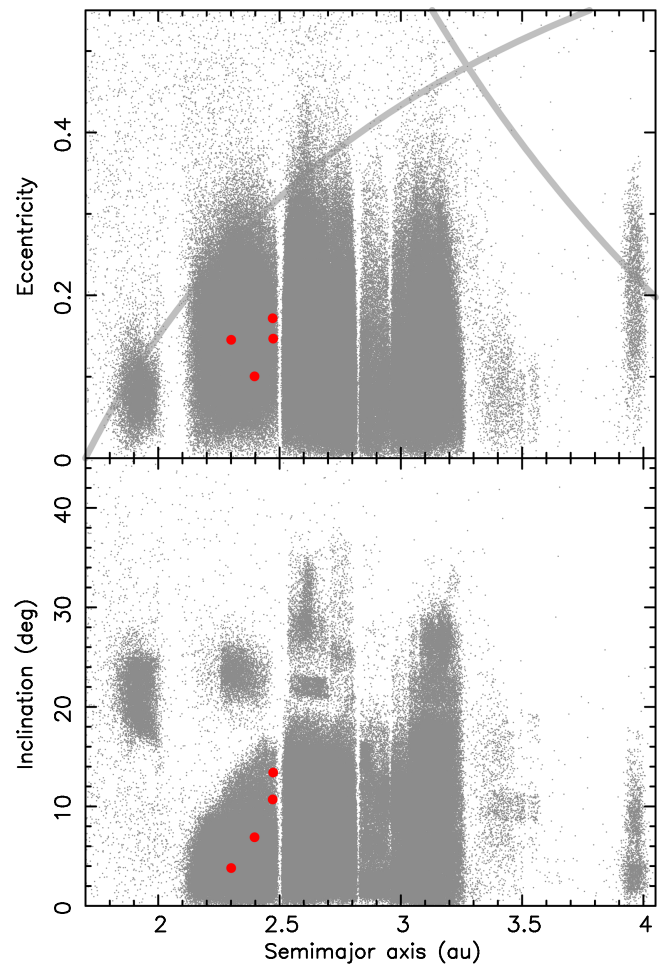


Figure 1. Orbits of numbered asteroids as of 2015 August shown in two-dimensional projections of the osculating element space: (i) semimajor axis vs. eccentricity (top), and (ii) semimajor axis vs. inclination (bottom). The red symbols indicate position of the four confirmed D-type asteroids by DeMeo et al. (2014). The gray lines at the top panel correspond to orbits with (i) perihelion equal to 1.7 au and (ii) aphelion equal to 4.85 au, which approximately delimit zones that are prone to destabilization by Mars and Jupiter. The Hilda asteroids with semimajor axes ≈ 3.95 au reside in the stable core of the J3/2 mean-motion resonance with Jupiter. As a result, they avoid close encounters with Jupiter and their orbits are long-term stable.

(Figure 1, and DeMeo et al. 2014), with the largest being ≈ 30 km in diameter, and only a handful of P-type asteroids with comparable or larger size. In contrast, there are more than 100 Trojan asteroids of this size (e.g., Emery et al. 2015). Henceforth, we assume that a factor of $\approx (20-30)$ more test planetesimals are needed in our simulations to potentially check our model results against constraints. Thus, because Nesvorný et al. (2013) used an equivalent of up to 50 million disk planetesimals, we need to increase this number to about a billion.

2.1. Phase 1: Planetary Instability

In accord with Nesvorný et al. (2013), our two selected NM12 case study simulations were denoted *Case1* and *Case2*. Figures 1 and 2 in Nesvorný et al. (2013) show the orbital histories of all of the giant planets participating in the instability for both cases, while here in Figures 2–7, we only show the more relevant orbits of Jupiter, Saturn, and the fifth ice-giant planet. In particular, Figures 2 and 3 show how the

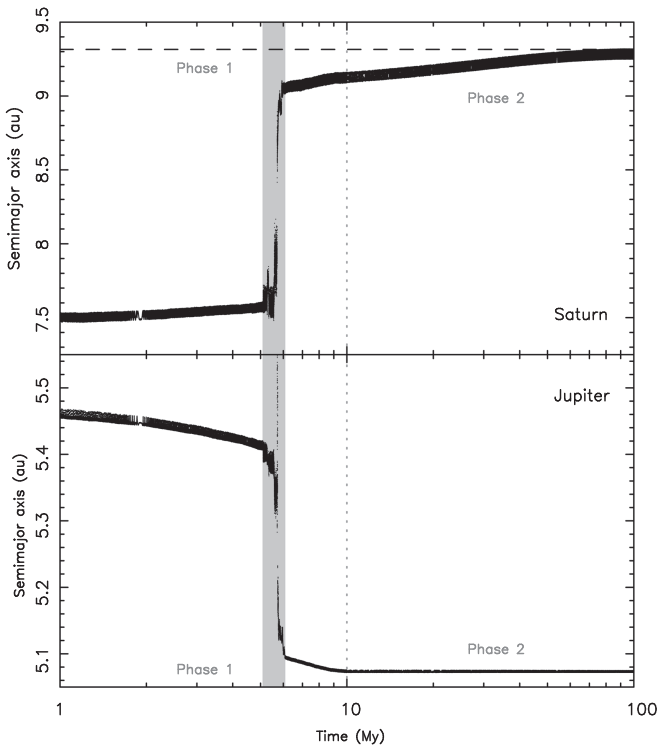


Figure 2. Time evolution of Saturn’s (top) and Jupiter’s (bottom) semimajor axis through phases 1 and 2 in the Case 1 simulation. Phase 1, lasting 10 Myr, accounted for the gravitational effects of 10,000 disk planetesimals initially placed in the trans-Neptunian region. Their gravitational effects made planets migrate slowly from their starting positions up to the moment of instability. The latter is very brief (gray box) and characterized by close encounters between giant planets. In particular, the abrupt jump in semimajor axis of both gas giants at ≈ 6.09 Myr is due to their interaction with the fifth giant planet that was consequently ejected from the planetary system. When the instability ends, an ordered and slower evolution of planetary orbits is restored. During phase 2, lasting 100 Myr, Jupiter and Saturn were slowly migrated into their final orbits in our simulation. At this phase, no direct gravitational effects due to planetesimals on planets were modeled; rather, fictitious weak accelerations in the planetary orbits were applied to make them reach pre-defined final orbits (see Section 2.2). The dashed horizontal line in the top panel shows Saturn’s position with respect to the Jupiter orbit with the observed period ratio ≈ 2.49 .

orbits of Jupiter and Saturn evolved before, after, and throughout the brief instability period (indicated by a gray rectangle). Figures 4–7 show the orbit evolution of the fifth planet where it is most relevant for our work, namely, what happened to it during the dynamical instability. The reader should note that particular attention should be paid to when its orbit was temporarily interior to that of Jupiter.

As in Nesvorný et al. (2013), we only used a portion of the full NM12 simulations that typically lasted 100 Myr. Our segment, which describes the orbital evolution of the planets a few My before and after the instability, is what we denote here as phase 1. In both Cases 1 and 2, the phase 1 simulations lasted 10 Myr, with the dynamical instability roughly in the middle of this interval.

Note that in the original NM12 simulations, planet–planet and planet–planetesimal interactions were modeled explicitly, but for computational expediency, the planetesimal disk was only represented by 10,000 particles. This number is much too small to provide us with useful estimates of the capture probabilities of trans-Neptunian disk planetesimals into small-body populations like the Jupiter Trojans, irregular satellites, or main-belt asteroids. For that reason, Nesvorný et al. (2013)

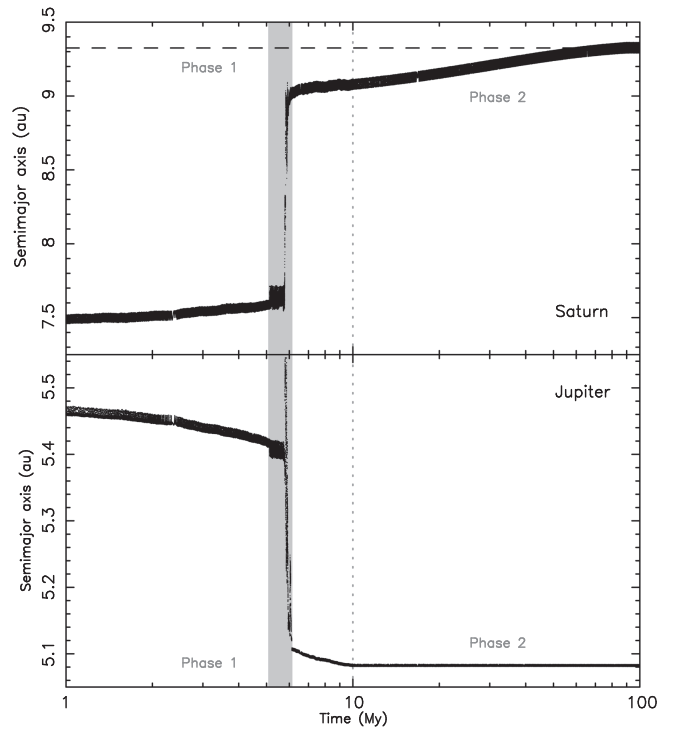


Figure 3. Same as in Figure 2, but now for Jupiter and Saturn in our Case 2 simulation.

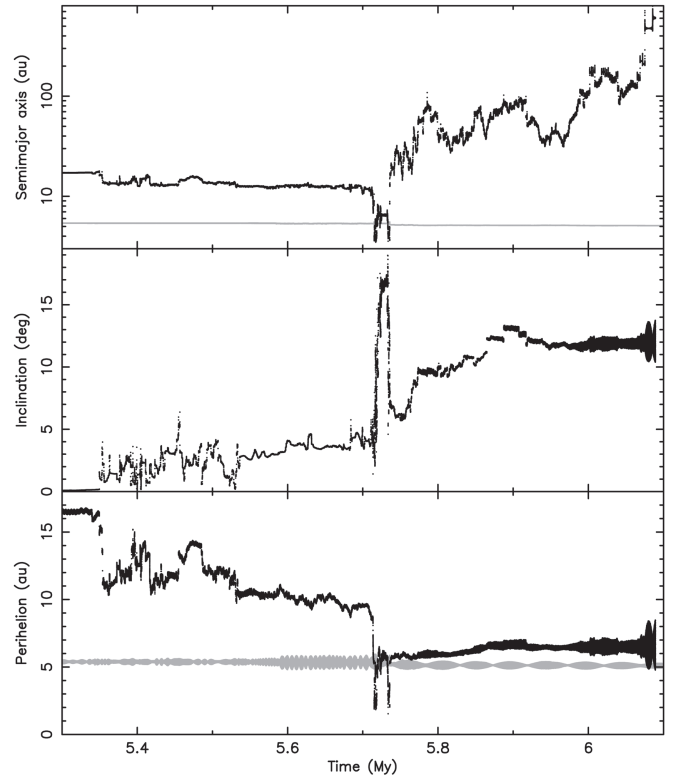


Figure 4. Orbital elements of the fifth giant planet in the Case 1 simulation during the interval of time it experienced strong interactions with other planets in the system: (i) semimajor axis (top), (ii) inclination (middle), and (iii) perihelion (bottom). The gray curve in the top panel is the semimajor axis of Jupiter and the gray zone in the bottom panel shows the range between perihelion and aphelion of Jupiter for comparison. The fifth planet was ejected as a consequence of Jupiter encounters at ≈ 6.09 Myr.

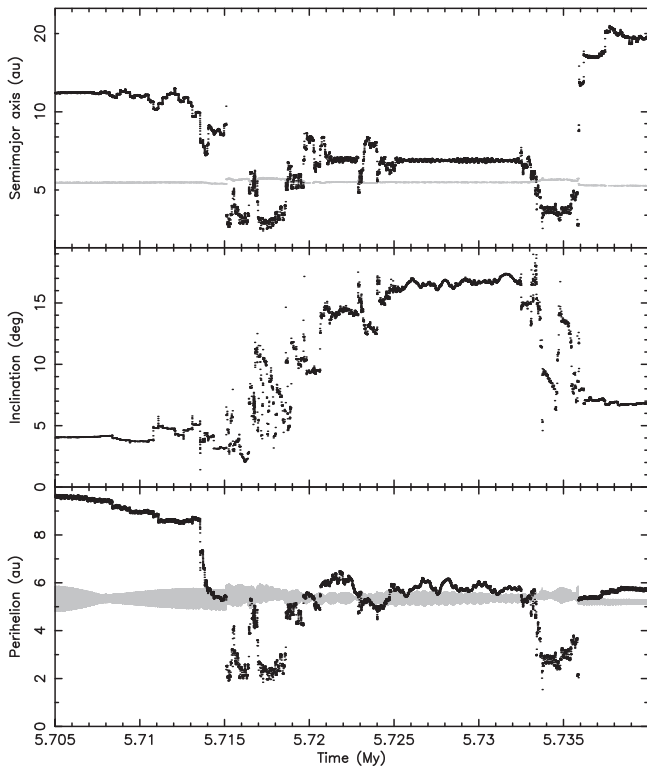


Figure 5. Zoom of the fifth-planet orbital evolution in the Case 1 simulation during a time period when its perihelion was mostly, and the semimajor axis occasionally, below Jupiter’s orbit (panels as in Figure 4). In this case, the period was rather brief, lasting only ≈ 30 kyr.

developed a new method in which the planetary orbits from the **NM12** runs are exactly reproduced, with their position and velocity state vectors stored in a file with an output timestep of 1 year. Even if compressed into a binary format, all of the data describing 10 Myr of phase 1 produced a nearly 2 gigabyte file. It was thus impractical to extend phase 1 to longer times.

In addition, while generally successful, the **NM12** simulations were not able to reproduce exactly the final orbits of the giant planet. This is an unfortunate circumstance; ideally, we want our simulations here to match the relative configuration of the giant planets as much as possible. In particular, we would like to determine the right orbits of Jupiter and Saturn because many objects are trapped in or affected by resonances under their influence. For this reason, we make use of the shorter phase 1 and then complement it with a new phase 2 period during which the planets are placed into their relative configuration more precisely than in the original **NM12** simulation. The new phase 2 period will be briefly described in Section 2.2.

Using the stored phase 1 planetary state vectors, we insert these data into a modified version of a well-tested integrator⁵ `swift_rmvs3`. This allows us to propagate any number of test disk planetesimals we choose during phase 1. Our modification replaces the actual swift-integration of massive planets, with their positions and velocities interpolated between timesteps to any time required by the numerical propagation of added test disk planetesimals, with the interpolation done in Cartesian space. In practice, we use an integration timestep of 0.2 years in phase 1. The test planetesimals were eliminated

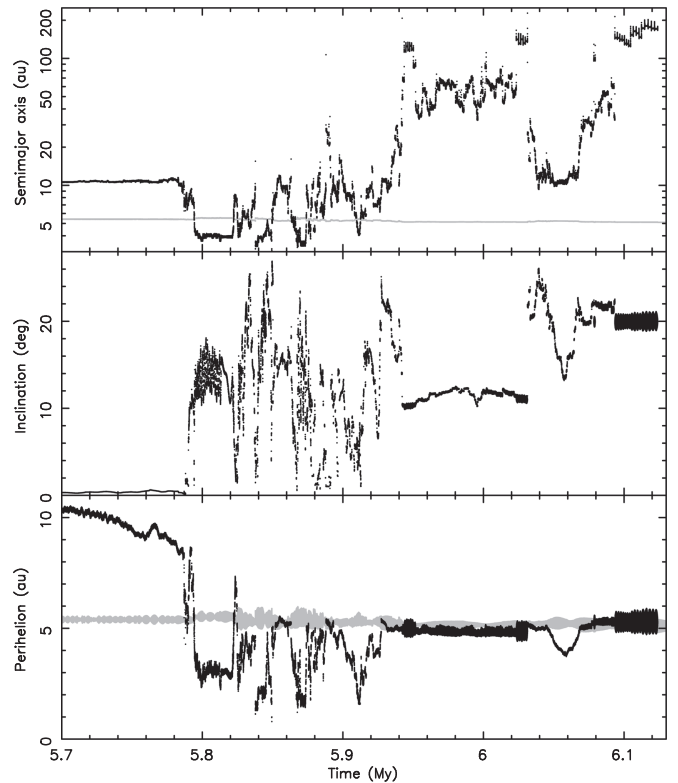


Figure 6. Orbital elements of the fifth giant planet in the Case 2 simulation during the interval of time in which it experienced strong interactions with other planets in the system: (i) semimajor axis (top), (ii) inclination (middle), and (iii) perihelion (bottom). The gray curve in the top panel is the semimajor axis of Jupiter and the gray zone in the bottom panel shows the range between perihelion and aphelion of Jupiter for comparison. The fifth planet was ejected as a consequence of Jupiter encounters at ≈ 6.14 Myr.

when they impacted one of the planets, they came within 0.1 au of the Sun, or they reached a distance of 1000 au from the Sun. This method allows us to run the same types of `swift_rmvs3` simulations on many different CPUs. Accordingly, we can simulate the evolution of numerous test planetesimals, yet be sure we always reproduce exactly the same and requested planetary orbits.

Our test planetesimals were initially distributed in a dynamically cold disk extending from ≈ 23 to 30 au. The inner edge was about 0.5 au beyond Neptune’s initial orbit. The surface density Σ of particles in the disk was set to $\Sigma \propto 1/r$, where r is the radial distance from the Sun. The eccentricity and inclination values of the planetesimal orbits had an initial Rayleigh distribution with variance equal to 0.01 and 0.005 rad, respectively. The secular angles and longitude in orbit were chosen randomly between 0° and 360° . The initial disk-particle data mimic those originally used by **NM12** for the planetary migration runs.

Despite our ability to distribute our simulation over numerous CPUs, and having access to NASA’s powerful Pleiades’s supercomputer, tracking a billion test planetesimals is still beyond the ability of our available computer resources. For this reason, we adopted the planetesimal “cloning” approach described in Nesvorný et al. (2013). We initially ran a smaller number of particles N_{tp} , and then we cloned them N_{clo} times when they had reached heliocentric distance $r = 8$ au. Our bodies started their evolution on nearly circular orbits well beyond Neptune. They were then destabilized by

⁵ www.boulder.swri.edu/~hal/swift.html

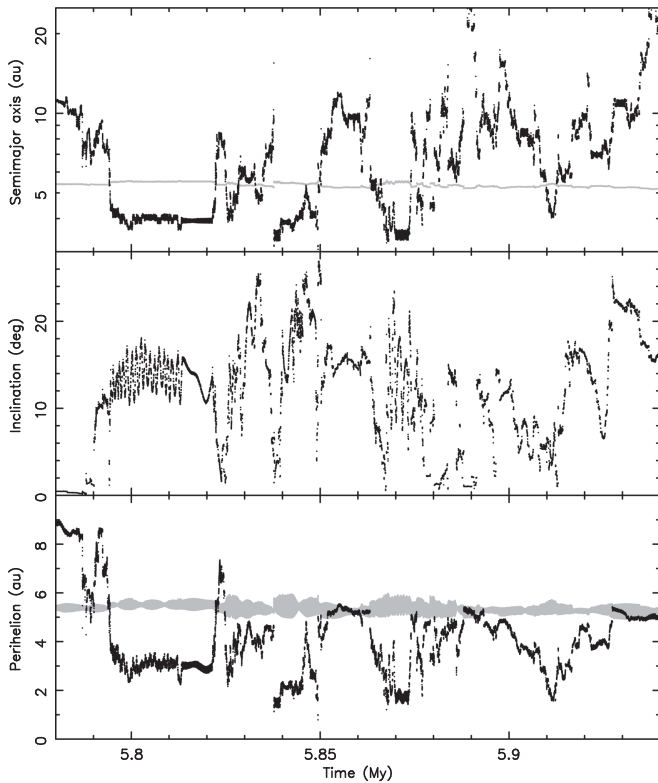


Figure 7. Zoom of the fifth-planet orbital evolution in the Case 2 simulation for a time period when its perihelion was below Jupiter’s orbit (panels as in Figure 6). In this case, the period was more extended and lasted nearly ≈ 140 kyr. The minimum perihelion distance values, reaching below 2 au, were also lower than in Case 1.

planetary perturbations. Many were delivered to orbits closer to the Sun where a tiny fraction could be captured on sub-Jupiter orbits.

The cloning was performed only once for each particle. The new bodies with given a minute change in velocity relative to the original body (fractionally changed by $\sim 10^{-8}$ at the moment of cloning). We found that the orbits quickly diverged because of strong gravitational perturbations by the giant planets. As a result, the total *effective* number of particles represented in our simulations was $N_{\text{eff}} = N_{\text{tp}} \times (N_{\text{clo}} + 1)$, with $N_{\text{clo}} + 1$ representing the number of clones; the original particle was kept in the simulation. We used $N_{\text{clo}} = 19$ and $N_{\text{tp}} = 50 \times 10^6$, such that $N_{\text{eff}} = 10^9$.

Our typical individual run initially had 2000 particles that increased to nearly 30,000 maximum running particles at some moment during the phase 1 simulation. With the above-mentioned number of N_{tp} , simulations for one of the two cases considered in this paper represented 25,000 individual jobs. This was a major effort, and the project lasted nearly a year of real time on our available computational resources. Additionally, given the enormous number of simulations, we were limited in our ability to closely track the orbital evolution of all of the particles during phase 1. This led us to choose a rather large output step of 0.5 Myr, which is just enough to monitor the broad-scale evolution of the particle cloud. Unfortunately, this sparse output frequency does not allow us to conduct a detailed study of the orbital evolution of individual particles.

2.2. Phase 2: Jupiter and Saturn Slowly Migrated to their Final Configuration

At the end of phase 1 in our simulations (i.e., at the 10 Myr epoch), we find that the four remaining planets are orbitally decoupled from one another. Their orbits were subject to a much slower evolution due to interactions with the last escaping remnants of the disk planetesimal population. This means that their planetary semimajor axes slowly change toward their final values, while their eccentricities and inclinations are slowly damped from possibly excited values by planetary encounters. The original NM12 simulations provide us with a hint concerning the relevant timescales, which turn out to be of the order of 30–100 Myr. This phase is more regular compared to the more dramatic phase 1, and so it is simpler to model. We call this time period *phase2*. In regard to our goal, we assume that the capture of disk planetesimals in the main belt zone from distant regions beyond planets all took place during phase 1, specifically, during the short period of planetary instability. Contributions from phase 2, and especially phase 3 (Section 2.3), were deemed to be negligible.

Planetary orbits during phase 2 were propagated forward using a modified `swift_rmvs3` integrator. Here, we include forces designed to mimic (i) the residual slow migration that takes place in the giant planets’ semimajor axes and (ii) giant planets’ damping in eccentricity. No meaningful changes were seen in inclination. The exact parametric formulation of the fictitious planetary accelerations, based on the earlier works of Papaloizou & Larwood (2000) and Papaloizou (2011), was given in Roig & Nesvorný (2015).

In order to speed up our computations, we also adopted the following two approximations. First, we discarded Uranus and Neptune from our simulations, continuing with only two gas giants, Jupiter and Saturn (see also Levison et al. 2009, who used the same approximation). We consider this acceptable because we are only interested in a small sub-population of test disk planetesimals that may eventually be captured onto sub-Jupiter orbits. Note that the dynamically stable region of the main belt is bracketed by (i) mean-motion resonances with Jupiter (and on a long-term carved out by three-body, mean-motion resonances with Jupiter and Saturn), and (ii) secular resonances defined by pericenter and node frequencies associated with Jupiter and Saturn (e.g., Knežević et al. 2002; Morbidelli 2002; Nesvorný et al. 2002). Perturbations due to the more distant planets Uranus and Neptune are less important. Note that bodies on orbits in the innermost part of the main belt may become unstable over long timescales via exterior mean-motion resonances with Mars. A related concern is the population of objects on low-inclination orbits; they could also become unstable if their perihelia were to become too close to Mars. We will deal with this effect separately in Sections 2.3 and 3.

In both Cases 1 and 2, Jupiter’s semimajor axis at the end of phase 1 was about 5.08 au (see Figures 2 and 3). This is one of the slight inaccuracies of the NM12 simulations. Here, we decided to not apply the fictitious acceleration that would lead to more semimajor axis migration for Jupiter. Instead, we only used it for Saturn. Saturn’s semimajor axis at the end of phase 2 was designed to correspond to the observed period ratio ≈ 2.49 of both gas giants.

Second, given the goals of our paper, we down-sampled the population of disk planetesimals, eliminating those that were on heliocentrically distant orbits which were unlikely to

contribute to main belt capture events. Therefore, at the beginning of phase 2, we only tracked planetesimals that resided on orbits that had the following values of osculating orbital elements: (i) semimajor axis smaller than 4.5 au, (ii) eccentricity smaller than 0.5, and (iii) inclination smaller than 50° . We consider our selection criteria to be very conservative. In fact, this set of bodies contained many unstable orbits that were eliminated by Jupiter’s perturbations over short time-scales.⁶ In this manner, we avoided losing potentially interesting test disk planetesimals. In both Cases 1 and 2, approximately 200,000 particles were tracked at the beginning of phase 2.

The phase 2 simulations were run for 100 Myr (Figures 2 and 3) using an integration timestep of 0.04 years. We also kept the same elimination criteria for the bodies as in phase 1, namely, removing them if (i) they hit Jupiter or Saturn or (ii) if their heliocentric distance was $r < 0.1$ au or $r > 1000$ au. Typically, we found that one-tenth of the particles that started at the beginning of phase 2 survived to the end of the simulations. This left us with 10,000–20,000 test disk planetesimals on quasi-stable, sub-Jupiter orbits.

2.3. Phase 3: Long-term Stability

Once the gas giants reached their final orbits, our fictitious accelerations were shut off. This defines the beginning of *phase3*. Here, we used the `swift_rmvs3` integrator and propagated Jupiter, Saturn, and all particles that reached the end of phase 2 for another 4 Gyr. This assumes that the planetary instability coincided with the late heavy bombardment some $\simeq 4.1$ Gyr ago (e.g., Bottke et al. 2012), although we do not expect major changes to occur if the instability was slightly older or younger.

The purpose of phase 3 was to probe the long-term orbital stability of the population of test disk planetesimals captured in the main belt. High-order and three-body mean-motion resonances with the planets can produce long-term instability, even in parts of the main belt which are safe from effects of the major resonances (e.g., Morbidelli 2002; Nesvorný et al. 2002). Phase 3 is mostly relevant for the outer main belt where we expect planetesimal deposition to be maximized. Note that the associated instability timescales range from hundreds of Myr to a Gyr, and thus a 4 Gyr simulation is well-justified.

In order to make our simulation in the phase 3 more efficient, we modified the elimination criteria for the test disk planetesimals. They are eliminated when they impact Jupiter, or when their heliocentric distance reaches $r < 1.5$ au or $r > 15$ au. The upper limit of 15 au is fairly conservative because it is impossible for bodies reaching larger heliocentric distances to achieve stable main-belt orbits. The lower limit of 1.5 au allowed us to remove a small number of test planetesimals that were left at the end of phase 2 on high-eccentricity, moderate- to high-inclination orbits. The reason we chose this lower cutoff was to model, in the crudest way, the effects of the terrestrial planets; they were not included in any phase of our simulations. Indeed, previous numerical experiments with inner main-belt orbits shows that as soon as the osculating perihelion becomes smaller than $\simeq 1.75$ au, the particles are on the pathway to being transferred to the

terrestrial planet-crossing zone (e.g., Morbidelli & Nesvorný 1999). So our elimination criterion is still conservative. We will consider individual test planetesimals when necessary in Section 3.

Our phase 3 numerical runs used a timestep of 0.04 days. About half of the particles started at the beginning of phase 3 were eliminated over 4 Gyr.

2.4. Additional Simulations

A specific task in our work is to understand the role of the fifth planet in the capture process of trans-Neptunian planetesimals into the main belt and the associated populations found in the first-order resonances with Jupiter. In order to explore this behavior, we used the architecture of the simulations discussed above, with modifications made to the phase 1 simulations in the following way.

Recall that the orbits of the giant planets are read from an input file, previously selected from among the `NM12` runs. This is also true for the planet masses, which increase very slightly because the `Symba` simulations used by `NM12` accumulate impacting planetesimals (e.g., Matter et al. 2009). In our phase 1 simulations, we only propagate test disk planetesimals in this pre-defined set of planetary orbits. As an approximate method, we can discard one of the planets from the simulation (for instance, by assigning it a “zero mass”). We applied this artificial modification to the case of the fifth planet and reran our Case 1 and Case 2 simulations. For computational expediency, we only ran the modified trials for $N_{\text{eff}} = 200 \times 10^6$ test disk planetesimals (as opposed to a billion before). The other planets, in particular, Jupiter and Saturn, behave exactly the same as before. This allows Jupiter to perform the needed jump from Figures 2 and 3 to preserve the architecture of the terrestrial planets.

3. RESULTS

We now summarize the results from our simulations. We first examine Case 1 (Section 3.1), followed by Case 2 (Section 3.2). The reason for separately discussing the two cases, which are just two possible realizations of the planetary dynamical instability in the `NM12` framework, is that they roughly bracket the expected results. In Case 1, the fifth planet experienced only brief visits to the sub-Jupiter orbital zone; most of its time was spent at larger heliocentric distances (Figures 3 and 4). Therefore, the effects of its perturbation on main-belt asteroids should be minimal. On the other hand, in Case 2, the fifth planet spent a much longer time in the sub-Jupiter zone and penetrated more deeply (Figures 5 and 6). Thus, the effects on main belt asteroids in this region may be significantly larger. In fact, Roig & Nesvorný (2015) were not able to find a satisfactory solution for Case 2 concerning the eccentricity and inclination distributions of the main belt. This was because the fifth planet stirred the main belt population too vigorously. These results, however, only became known to us after we performed most of our simulations. Regardless, Case 2 allows us to glean insights into the nature of end-member studies (i.e., those that could potentially succeed if planetary encounters were slightly less deep).

3.1. Case 1

Figure 8 shows the osculating orbital elements of test disk planetesimals selected at the end of phase 1 to continue on to

⁶ Note, however, that we could not use our simulations presented here to increase the statistics of captures into the population of Jupiter Trojans (see Nesvorný et al. 2013). While interesting, we save this task for a forthcoming study.

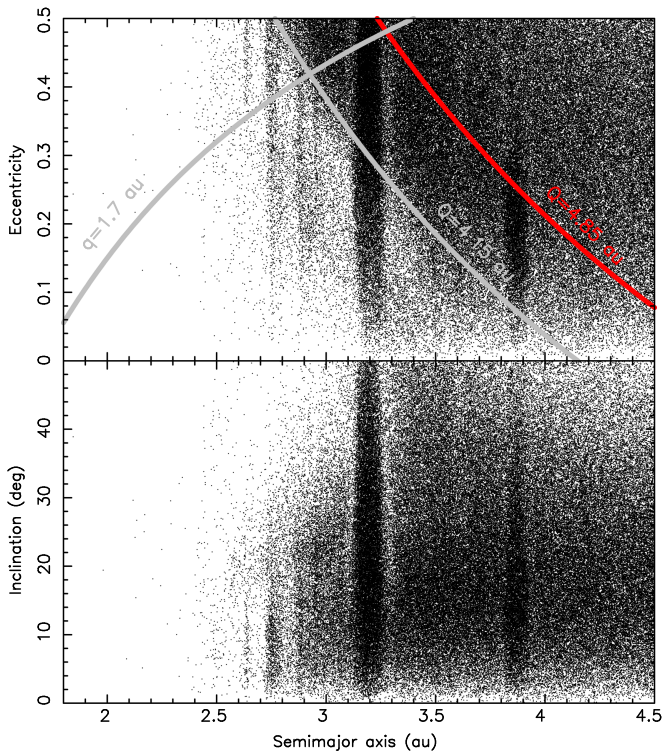


Figure 8. Osculating orbital elements, semimajor axis vs. eccentricity (top) and semimajor axis vs. inclination (bottom), of particles selected to continue at the beginning of phase 2 of our Case 1 simulation. About half of the particles reside in powerful, low-order, mean-motion resonances with Jupiter (such as J3/1, J2/1 or J3/2), while the remaining population was scattered onto orbits partially overlapping with the main-belt zone. Many of them that have aphelion larger than $\simeq 4.85$ au, as indicated by the red line, will be swiftly eliminated in phase 2 by close encounters with Jupiter. A denser concentration of particles continues to aphelion distance $\simeq 4.15$ au (gray curve at the top), which is roughly correlated with the deepest semimajor axis to which the fifth planet jumped (Figure 5). Orbits with perihelion smaller than $\simeq 1.7$ au (gray curve at the top) would be eliminated by close encounters with terrestrial planets, and they are eliminated during our phase 3.

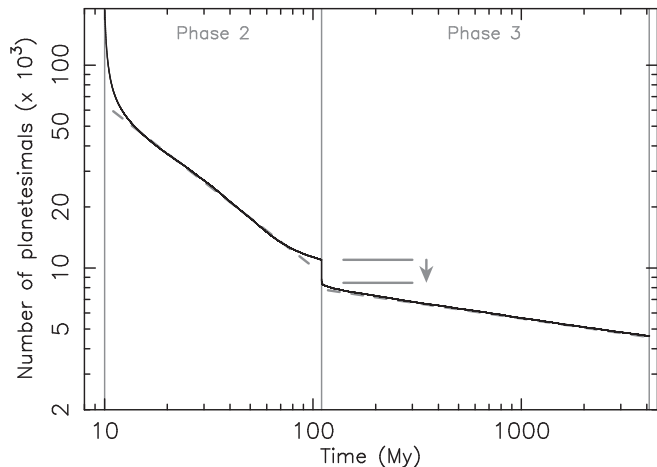


Figure 9. Number of particles remaining in the Case 1 simulation through phases 2 and 3 (solid line). Each of the two phases shows transient phenomena at the beginning: (i) many particles have been left on very unstable orbits at the beginning of phase 2 (Figure 8) and these were swiftly scattered by Jupiter, and (ii) orbits with $q < 1.5$ au and $Q > 15$ au were instantly removed at the beginning of phase 3 by our tightened elimination criteria, producing a drop in the population number. The dashed lines are power-law approximations $N \propto t^{-\alpha}$ with exponents of $\alpha \simeq 0.8$ in phase 2 and $\alpha \simeq 0.15$ in phase 3.

phase 2. As described above, we purposely remained conservative and selected a pool of orbits that largely encompasses those currently observed in the main belt (Figure 1). Many orbits with aphelion $Q > 4.85$ au (red line) are too close to Jupiter and will be scattered out of the Solar System on a short timescale at the beginning of phase 2.

We find that the density of orbits in semimajor axis versus eccentricity remains roughly constant down to $Q \simeq 4.15$ au (gray line). This value is approximately the smallest semimajor axis value occupied by the fifth planet before being scattered by Jupiter (Figure 5). A number of test disk planetesimal orbits are located in mean-motion resonances with Jupiter, most notably J2/1 and J3/2. Those that survive the subsequent orbital evolution will contribute to the stable populations found today in these resonances. Weaker, higher-order resonances with Jupiter are also temporarily populated by particles, but these will be dynamically eliminated over time.

A smaller number of bodies are scattered across the asteroid belt where they are not clearly associated with any mean-motion resonances. Unfortunately, our sparse output sampling during phase 1 does not allow us to track the detailed orbital histories of these particles. Nevertheless, we believe that many of them reached their orbits by the following two processes. First, they were transported close to their existing orbits within resonances associated with Jupiter. Next, some of them interacted with either secular resonances located inside the mean-motion resonances or chaotic layer associated with the resonance separatrix such that their eccentricities and inclinations began to have large excursions from the initial values. In this way, the bodies may become decoupled from Jupiter even at aphelion of their orbit. Finally, as Jupiter and the fifth planet were perturbed and experienced mutual jumps, these bodies dropped out of resonances. It is also possible that some bodies were injected into the main belt via close approaches with the fifth planet. Note that a few bodies are found to reside on orbits with perihelion $q < 1.7$ au (gray line). In reality, however, these bodies would have been destabilized by the gravitational effects of terrestrial planets. We will deal with this sub-population in phase 3 of our runs.

The dynamical decay of the number of test disk planetesimals through phases 2 and 3 is shown in Figure 9. Each of the phases has an initial drop in the population: (i) the phase 2 drop is due to the ejection of unstable particles on Jupiter-crossing orbits (see Figure 8), while (ii) the phase 3 drop is due to our new and more stringent elimination conditions for the bodies ($q < 1.5$ au and $Q > 15$ au). Except for these transient effects, each phase has intrinsic population decay dynamics that are roughly matched by a power law, $N(t) \propto t^{-\alpha}$. Phase 2 is characterized by a steeper exponent $\alpha \simeq 0.8$. Here, planetary orbits slowly evolve, with disk planetesimal instability driven by sweeping secular and mean-motion resonances. Phase 3 has a shallower exponent $\alpha \simeq 0.15$. Here, the planets have been “parked” onto their final orbits, such that the losses are driven by slow chaotic diffusion of those bodies trapped in mean-motion resonances. The population decreases by slightly more than a factor of 2 over the last 4 Gyr of phase 3, which is comparable to those of Levison et al. (2009). Table 1 contains basic quantitative information about our simulations as well as a summary of the final results.

A summary of our results at the end of phase 3 is shown in Figure 10. The left panels show the observed main-belt population (and the resonant objects) as they stand today as a

Table 1
Statistics of Planetesimal-capture Simulations onto Sub-Jupiter Orbits

	Case 1	Case 2
N_{eff}	10⁹	10⁹
$N_{\text{phase 2}}$	186,988	224,413
$N_{\text{phase 3}}$	10,976	21,013
N_{final}	4610	9603
N_{inner}	5	37
N_{central}	293	1240
N_{outer}	2372	5769
N_{Cybele}	1214	1505
$N_{\text{J2/1}}$	57	173
$N_{\text{J3/2}}$	668	877
$N_{\text{J4/3}}$	1	2

Note. Summary of results for the two Cases: N_{eff} is the effective number of simulated planetesimals initially in the trans-Neptunian disk (see Section 2.1), $N_{\text{phase 2}}$ number of planetesimals at the beginning of phase 2, $N_{\text{phase 3}}$ number of planetesimals at the beginning of phase 3, N_{inner} number of planetesimals implanted onto orbits below the J3/1 resonance (inner main belt), N_{central} number of planetesimals implanted onto orbits in between the J3/1 and J5/2 (central main belt), N_{outer} number of planetesimals implanted onto orbits in between the J5/2 and J2/1 resonance with Jupiter (outer main belt), N_{Cybele} number of planetesimals implanted onto orbits beyond the J2/1 resonance (Cybele zone), $N_{\text{J2/1}}$ number of planetesimals implanted onto orbits in the J2/1 resonance (Zhongguo population), $N_{\text{J3/2}}$ number of planetesimals implanted onto orbits in the J3/2 resonance (Hilda population), $N_{\text{J4/3}}$ number of planetesimals implanted onto orbits in the J4/3 resonance (Thule population). The number of Cybele objects N_{Cybele} also contains the high-eccentricity and high-inclination population in the Kozai resonance (see Section 3.1.3). The bold values denote initial and final total number of planetesimals.

function of osculating semimajor axis versus eccentricity and semimajor axis versus inclination. The right panels show all of our captured test disk planetesimals: 4610 in all. Most captured bodies are located beyond $a > 2.5$ au, which is similar to the results of Levison et al. (2009). Additional insights into the orbital structure of the captured population can be found in Figure 11. Here, the lower panel shows orbital aphelion of the implanted bodies versus their orbital inclination.

The most noticeable feature of the captured orbits in Figure 10 is a tendency for bodies with lower semimajor axis to have higher eccentricities (top and right panel). Figure 11 indicates that this correlation proceeds along the a line of constant aphelion. This relationship may help us to understand the capture mechanism. As mentioned above, we speculate that the planetesimals interact with mean-motion and secular resonances with Jupiter, temporarily populating their location. As the fifth giant planet cruises through their orbital zone, some have close encounters that kick them out of the resonance through a small jump in semimajor axis (this mechanism has been observed also in simulations of Roig & Nesvorný 2015). The top panel of Figure 11 shows the zone of heliocentric distance visited by the fifth planet during its instability phase. The aphelion region of the captured planetesimals coincides with this zone (note that its perihelion and aphelion distances are less effective because the planet had non-negligible inclination in the monitored time interval; Figure 5). Therefore, planetesimals whose aphelion values cross the path of the fifth planet can be efficiently deposited into the main belt.

Examining the details, we find the following results. On quantitative grounds, we will use the planetesimal population count compiled in Nesvorný & Vokrouhlický (2016). They

estimated the likely size frequency distribution in the primordial trans-Neptunian disk to be between $\simeq 23$ and 30 au (used in our simulations). We assume that the uncertainties on these values are at least a factor of 2. By combining these values with the capture probability from our simulations, we can estimate the captured population. This will allow us to compare our results with a census of D- and P-type objects in different main belt zones.

3.1.1. Capture Results for Disk Planetesimals between 2.1 and 2.5 au

We found that five bodies were captured onto orbits in the inner main belt between 2.1 and 2.5 au (i.e., semimajor axis smaller than that of the J3/1 resonance at 2.5 au). Their orbits are located between 2.3 and 2.5 au. These values are consistent with 10 of the 11 P/D-type asteroids in the inner main belt with $D > 30$ km (e.g., DeMeo et al. 2014; F. DeMeo 2016, personal communication). The exception to this is (336) Lacadiera, a $D \sim 70$ km P-type located at $\simeq 2.25$ au. Note that Levison et al. (2009) argued that this body had an unusual spectra which may be a poor fit for the P/D class.

We find the approximate capture probability for this zone to be $\simeq 5 \times 10^{-9}$ per test disk planetesimal. Assuming that the primordial disk has 5×10^8 $D > 30$ km objects, with factor of 2 uncertainties, we find that the largest P/D-type asteroid should be 50 ± 20 km in diameter. This range is a reasonable match to the sizes of the four largest P-types: (304) Olga, with $D \simeq 72$ km; (336) Lacadiera, with $D \simeq 69$ km; (248) Lameia, with $D \simeq 56$ km; and (474) Prudentia, with $D \simeq 43$ km (F. DeMeo 2016, personal communication). The largest confirmed D-type is (908) Buda, which has $\simeq 30$ km, although (732) Tjilaki, with $D \simeq 40$ km, is also a D-type candidate (DeMeo et al. 2014).

Our model predicts 3 ± 2 $D > 30$ km P/D-types objects captured in the inner part of the main belt. Assuming that the observed number is of the order of 10, and all objects here have been classified correctly, then our prediction is too low by a factor of ~ 3 , although the uncertainty range is between 2 and 10. Interestingly, this mismatch, when combined with insights from our Case 2 results, may be telling us that the fifth giant planet needs to spend a little longer below Jupiter's orbits than in Case 1 and a little shorter than in Case 2. We will return to this issue in the Discussion section.

3.1.2. Capture Results for Disk Planetesimals between 2.5–2.8 au and 2.5–3.6 au

Many more test disk planetesimals were captured into the central and outer main belts. In Case 1, 293 test disk planetesimals were captured between the J3/1 and the J5/2 resonances ($2.5 < a < 2.82$ au), 2372 bodies were captured in the central and outer main belt between the J5/2 and J2/1 resonances ($2.5 < a < 3.25$ au), and 1214 bodies were captured beyond the J2/1 mean-motion resonance with Jupiter in what is called the Cybele population ($\simeq 3.25 < a < 3.6$ au). This means that the capture efficiencies per test disk planetesimal for $2.5 < a < 2.82$ au, $2.5 < a < 3.25$ au, and $2.5 < a < 3.6$ au are $\simeq 3 \times 10^{-7}$, $\simeq 2.7 \times 10^{-6}$, and $\simeq 3.9 \times 10^{-6}$, respectively. These values are smaller than, but comparable to, what was reported by Levison et al. (2009).

Our goal was to compare these data to the largest P/D types found in each region; they are the least likely to have

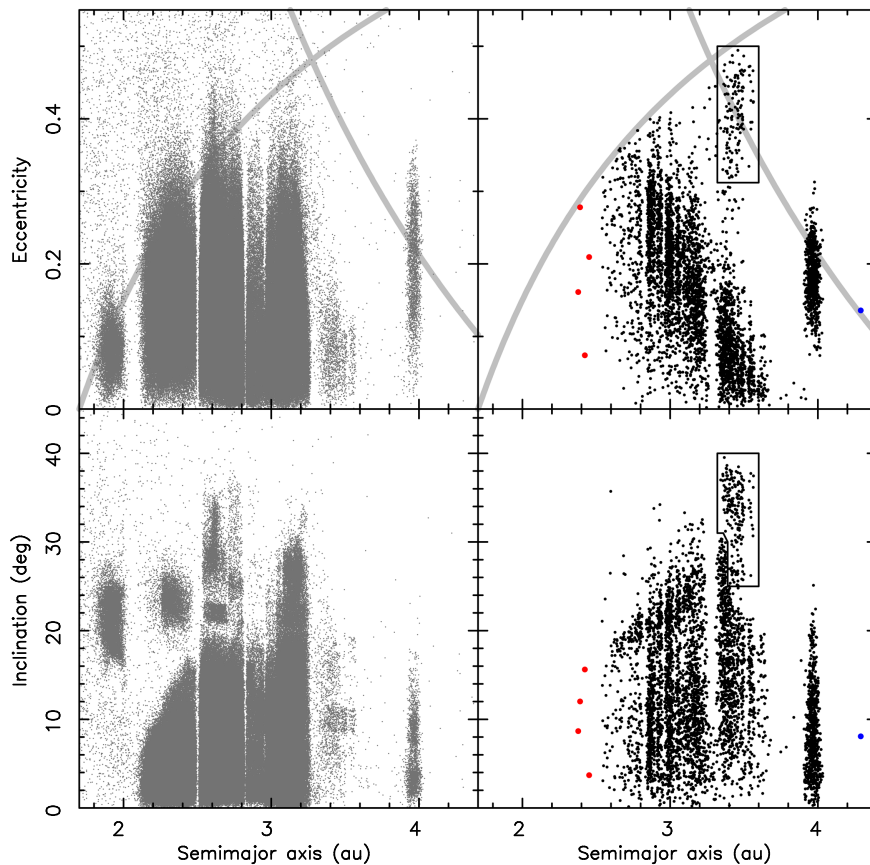


Figure 10. Particles in the main-belt, Hilda, and Thule orbital zones that remained in the Case 1 simulation at 4 Gyr (right column) compared with the observed population of asteroids (left column; see also Figure 1). Top panels show semimajor axis vs. eccentricity (gray lines as in Figure 1), bottom panels show semimajor axis vs. inclination. The red symbols highlight particles interior to the J3/1 mean-motion resonance with Jupiter. The blue symbol is one particle resident in the stable zone of J4/3 mean-motion resonance with Jupiter. The rectangle/polygon in the right panels indicates the population of particles captured in Kozai states in our simulation (see discussion in the main text).

experienced substantial collisional evolution over 4 Gyr. We did this by multiplying the capture efficiencies above to the planetesimal population from Nesvorný & Vokrouhlický (2016), with factor of 2 uncertainties assumed.

1. $2.5 < a < 2.82$ au; *large asteroids*: We predict that the largest P/D type in this zone should have a diameter of 180 ± 25 km. This agrees with the diameter of (409) Aspasia, which is $D \simeq 177$ km and has $a \simeq 2.58$ au (F. DeMeo 2016, personal communication). Similarly, assuming that there were $\simeq 5 \times 10^7$ $D > 150$ km bodies in the primordial disk, we estimate that there should be 20^{+20}_{-10} $D > 150$ km bodies. From the estimates of F. DeMeo (2016, personal communication), there are ~ 17 P/D-types that are $D > 150$ km, a good match.
2. $2.5 < a < 3.6$ au; *large asteroids*: We predict that the largest implanted object should have a diameter between 260 and 350 km. This agrees with the size of (65) Cybele, which is 301 ± 5 km (Kasuga et al. 2012) or $302 \times 290 \times 232$ km (Müller & Blommaert 2004), and (87) Sylvia, a P-type asteroid that is $D \simeq 263$ km (Kasuga et al. 2012). Sylvia also has a family associated with it created by a large cratering event (Vokrouhlický et al. 2010), such that Durda et al. (2007) estimated the original parent body to be $D \simeq 270$ km. For $D > 150$ km bodies, we predict that there should be 29^{+29}_{-14} of them, while the

observed number is ~ 15 . Our model value agrees within the lower bound.

For smaller asteroids, we turn to the main-belt size frequency distribution estimated using *WISE* infrared data (Masiero et al. 2011). They find that there are about 1400 and 5500 $D > 10$ km asteroids in the central and outer main belt, respectively, where they define the central main belt to be between J3/1 and J5/2, while their outer main belt is between the J5/2 and 3.6 au. Data compiled by DeMeo & Carry (2014) suggest that there are $\simeq (10\text{--}20)\%$ dark objects with steep spectra in this orbital zone; this represents regrouping the P/D-types together, something suggested by the census of the Hilda and Trojan populations (see also DeMeo et al. 2015). Thus, our target number is approximately 700–1400 P/D-types with $D > 10$ km. For the region between 2.5 and 2.82 au, there should be 140–280 such bodies. If we assume that there were $\simeq 4 \times 10^9$ $D > 10$ km objects in the primordial disk, then we would expect that about $16,000 \pm 8000$ $D > 10$ km P/D types should have been implanted into the outer main belt (2.5–3.6 au region). This fraction is of the order of a factor 10 more than the observed population.

There are many potential reasons for the mismatch on the low size end. While commenting in more detail on these reasons in Section 4, we mention here (i) the observational incompleteness of the main belt population in terms of identifying P/D types, (ii) the elimination of planetesimals

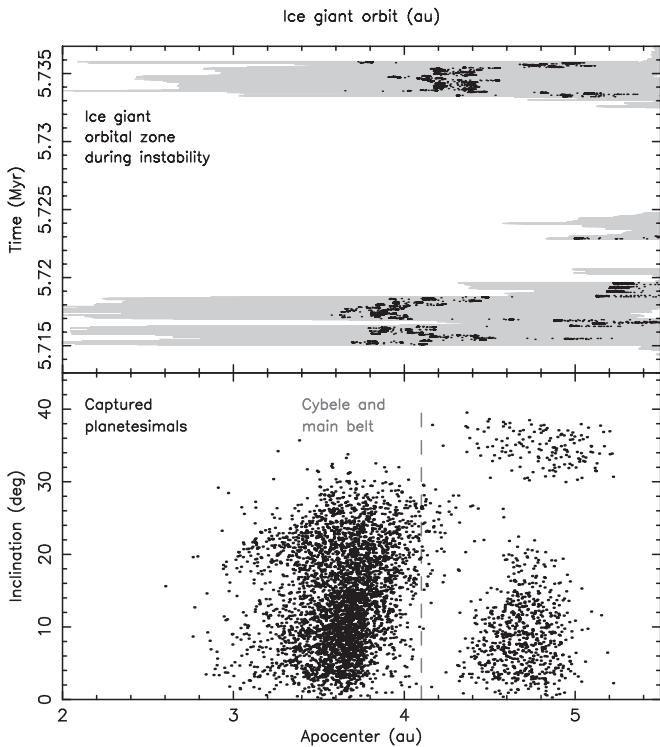


Figure 11. Bottom part: same as in the right panels of Figure 10, with the orbits of planetesimals permanently captured onto the sub-Jupiter orbits, now shown as apohelion distance Q (abscissa) vs. inclination I (ordinate). The two groups with $Q > 4.1$ au are Hildas (low- I case) and the Kozai librators highlighted in Figure 10 by a rectangle (high- I case). Orbits with $Q < 4.1$ au are Cybeles and main belt objects. Top part: heliocentric orbital zone reached by the fifth giant planet during the core of the instability period: time (ordinate) as on Figure 5 vs. semimajor axis (black symbols). The gray zone is the difference between perihelion and aphelion; note the upper abscissa. Comparison of the data in the two panels suggests that planetesimals are most efficiently deposited onto orbits whose aphelion reaches to the zone visited by the fifth planet.

transported from heliocentrically distant regions by thermal or volatile-driven bursting during their deposition into sub-Jupiter zone, which may be a function of size, (iii) collisional destruction (Levison et al. 2009), or (iv) the resonance escape of bodies via Yarkovsky thermal drift over 4 Gyr (Bottke et al. 2006 and Section 4). We believe a combination of these effects may provide the needed “mismatch factor” of $\simeq 10$.

3.1.3. Dynamical State of the Cybele Population

Examining the dynamical state of our simulated Cybele population in more detail, we find that they typically have low eccentricity and small to moderate inclination orbits. These values are consistent with the conditions of long-term stability studied by several authors using analytical techniques and numerical methods (e.g., Milani & Nobili 1985; Holman & Murray 1996; Murray & Holman 1997). These authors found that a dense network of high-order, mean-motion resonances is responsible for clearing most of this zone over a billion year timescale. Additionally, Liou & Malhotra (1997), and later Minton & Malhotra (2009, 2011), argued that further destabilization of the zone is achieved by sweeping of the mean-motion and secular resonances as Jupiter migrated into its final position. Similar results were recovered within the framework of the five-planet scenario by Roig & Nesvorný (2015), who found most of this zone to be cleared at the end of their simulation.

Interestingly, there is a small population of 143 orbits in our simulation output, all adjacent to the J2/1 resonance with large eccentricities and inclinations (see the orbits inside the rectangle/polygon in the right panels of Figure 10). These orbits are lucky survivors from a vast population of planetesimals with similar orbits seen at the beginning of phase 2 (see Figure 8). Because many of these bodies formally have $Q > 4.9$ au, we paid closer attention to their orbits. Extending the phase 3 test disk planetesimal integrations by an additional 500 kyr, we found that all of these “anomalous orbits” happen to be captured in a Kozai state (see Kozai 1962). This means that their argument of pericenter circulates about 90° or 270° (Figure 12; note that the orbit of asteroid (1373) Cincinnati has similar behavior to the red orbit in this figure). This protects the body from having close encounters with Jupiter since the nodal heliocentric distance is always $\simeq a(1 - e^2) \simeq 2.8$ au.

While interesting, there is no similar group of notable bodies among the known asteroids; (1373) Cincinnati is but a rare example.⁷ Obviously, strong observational biases work against the discovery of these bodies. We suspect, however, that some details in our Case 1 model are inaccurate, and that this orbital zone is susceptible to a mismatch. For example, while the orbits of Jupiter and Saturn have the correct mutual ratio of their orbital periods, our Jupiter is about 0.1 au closer to the Sun than its actual orbit (this is the outcome of phase 1). As a result, the secular frequencies of the Jupiter–Saturn pair are not exact, as shown in Figure 13. Additionally, as computed in Knežević et al. (1991), the lower-frequency secular modes related to ice giants, namely, g_7 , g_8 , s_7 , and s_8 , may help clear this zone, but they are not present in our simulation.

3.1.4. Capture of Disk Planetesimals in the Hilda Population (J3/2 Resonance)

We paid particular attention to the populations of planetesimals captured into the first-order, mean-motion resonances with Jupiter (e.g., Nesvorný & Ferraz-Mello 1997). Figure 8 suggests that these resonances are important capture gateways for trans-Neptunian planetesimals in the sub-Jupiter orbital zone. One should consider, however, that it takes another 4 Gyr of evolution to reach the current epoch, during which many of these bodies may be dynamically removed.

To test the number of objects that survived in the first-order, mean-motion resonances with Jupiter, we extended the phase 3 simulation by an additional 250 kyr, saving our output every 5 years. We then followed each of the 4610 particles and monitored the behavior of the resonant angles $\sigma_p = (p + 1)\lambda_J - p\lambda - \varpi$, where λ_J is the mean longitude of Jupiter, λ is the mean longitude of the particle, and ϖ is its longitude of pericenter. We tested $p = 1, 2$, and 3. Resonant particles are characterized by the libration of σ_p over a limited range of values, typically about 0° .

The most notable of these sub-populations is the Hilda population in the J3/2 resonance near 4 au. We recorded 668 planetesimals captured into this zone in Case 1. Figure 14 shows the distribution of libration amplitude of the resonant angle σ_2 . As expected, the chaotic capture produces a population that randomly samples the available, long-term stable region in the resonance. Therefore, the distribution of σ_2

⁷ We find it symbolic that this exceptional orbit was the only asteroid discovery of Edwin Hubble.

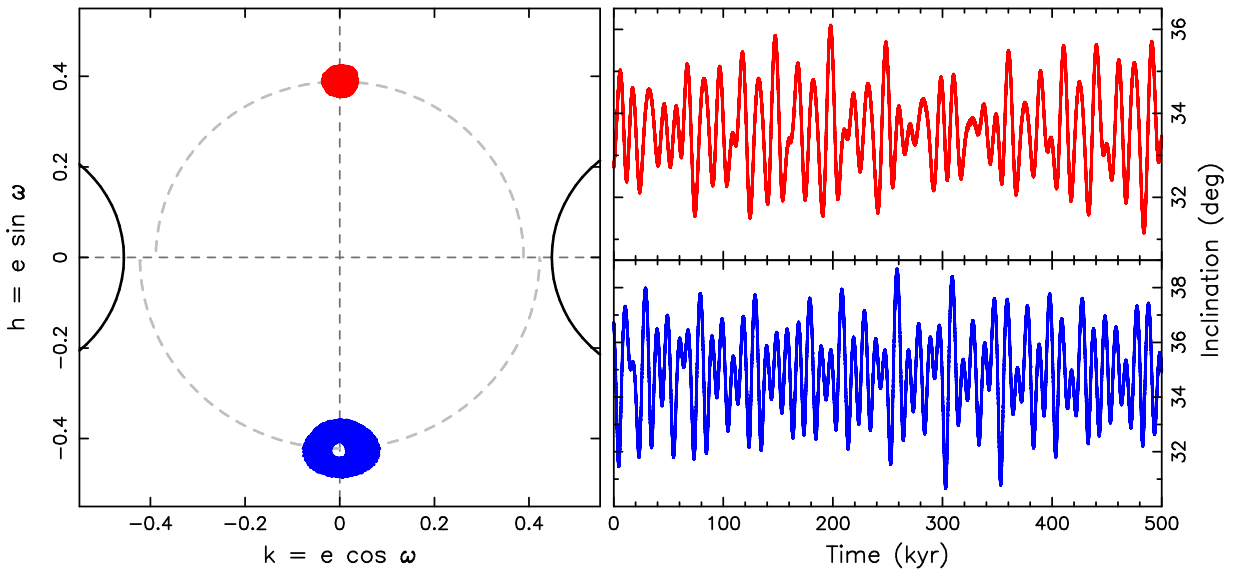


Figure 12. Two examples of orbits from the high-eccentricity and high-inclination Cybele population captured in our simulations. Left panel shows the evolution projected into the plane of non-singular elements $k + ih = e \exp(i\omega)$, where e is the orbital eccentricity and ω is the argument of pericenter. Symbols show evolution of the osculating orbital elements during 500 kyr time interval. Both orbits (red and blue symbols) are captured about the off-center stationary points of the secular evolution described by Kozai model. The solid circles define intersection with the ecliptic circular orbit of heliocentric radius 4.85 au (right circle for the red trajectory, left circle for the blue trajectory; note that both have a slightly different value of mean semimajor axis). Right panels show time evolution of the orbital inclination of both orbits.

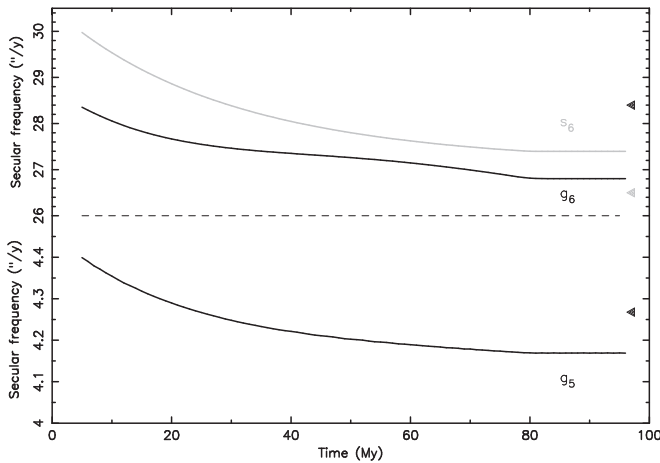


Figure 13. Evolution of the principal secular frequencies of the Jupiter–Saturn system during the 100 Myr of the phase 2 in the Case 1 simulation (the high-frequency sector at the top, the low frequency sector at the bottom, separated by the dashed line). All frequencies decrease as the planets slowly migrate away from each other (Figure 2). The nodal frequency, denoted s_6 for its easier identification with that in the real planetary system, is shown by a gray line at the top panel. The pericenter frequencies are accordingly denoted g_5 (lower) and g_6 (higher). The values were determined by Fourier analysis of the planetary orbital evolution using a 10 Myr wide sliding interval in time. The exact values in the solar system—indicated by the triangle symbols—read: $g_5 \simeq 4.25$ arcsec yr $^{-1}$, $g_6 \simeq 28.24$ arcsec yr $^{-1}$, and $s_6 \simeq -26.34$ arcsec yr $^{-1}$.

is quite broad, extending up to $\simeq 120^\circ$. If compared to the distribution of the same quantity for large Hildas, the dashed line in Figure 14 and also Figure 2 in Franklin et al. (2004), then we find that our distribution lacks objects on small σ_2 values (roughly $\sigma_2 \leq 40^\circ$).

The reason for this small mismatch, though not quantitatively modeled here, may be understandable. The Hilda population is a mixture of captured trans-Neptunian planetesimals (P/D-type bodies) and asteroids possibly born in situ (the C-type sub-population). While Roig & Nesvorný (2015)

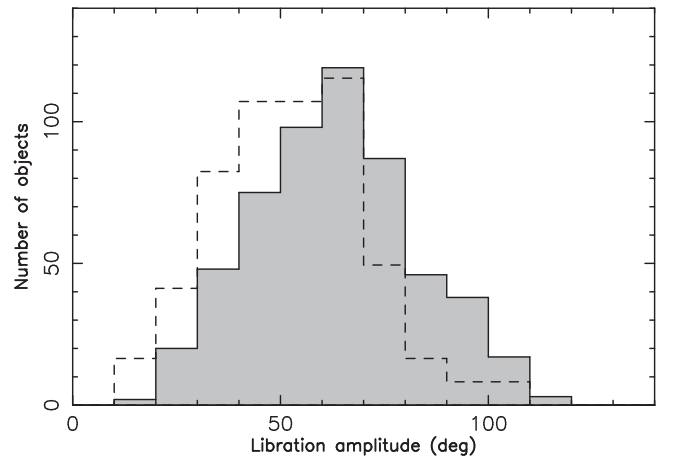


Figure 14. Distribution of libration amplitudes of planetesimals captured in the Hilda population (J3/2 mean-motion resonance with Jupiter) in our Case 1 simulation—gray histogram. Dashed line shows the same for 100 largest Hilda asteroids (in order to compare the two we recalibrated their total number to be 668 as in the simulated sample). In both cases we integrated the orbits for 250 kyr and computed maximum and minimum values of the resonant angle $\sigma_2 = 3\lambda_J - 2\lambda - \varpi$; reported libration amplitude at abscissa is half the difference between these extremal values.

verified that the majority of Hilda asteroids were captured during the planetary instability phase, their initial orbits were quite different from those in the exterior disk. Thus, the final orbits in the resonance might be more tightly concentrated toward the libration center. This contrasts with the captured population from the trans-Neptunian disk modeled in this paper which prefers filling the phase space of stable orbits in the J3/2 resonance uniformly.

The large end of the Hilda’s size frequency distribution can be predicted using the size frequency distribution from Nesvorný & Vokrouhlický (2016) and a capture probability of $\simeq 7 \times 10^{-7}$ per test disk planetesimal. We predict that the largest Hilda should be $D \simeq 180\text{--}240$ km. This range is

comparable to the size of (153) Hilda, which has a diameter of $\simeq 170$ km. Like Sylvia, (153) Hilda also has a family. Reconstructing the size of the parent body, Brož & Vokrouhlický (2008) and Brož et al. (2011) calculated that it was originally $D \simeq 200 \pm 20$ km. This agrees well with our estimates. For $D > 150$ km bodies, we predict that there should be 5^{+5}_2 of them, while the observed number is ~ 3 . Our model value once again agrees within the lower bound.

For smaller asteroids, we find that there are slightly more than 1000–1500 $D > 10$ km Hilda asteroids (e.g., Grav et al. 2012a, 2012b), with about 70%–80% of them having steep spectra consistent with P/D-types (see DeMeo & Carry 2014). Therefore, a population of about 700–1200 captured planetesimals among Hilda asteroids would be compatible with the observations. Instead, we predict $\simeq 2800$ bodies. The mismatch factor here is only 3–4. We hypothesize that this difference may have to do with the fact that some of the above proposed mechanisms (such as the Yarkovsky-driven elimination) are ineffectual in the Hilda zone. If so, then observational incompleteness and collisional evolution may be enough to explain the difference.

In this respect, we find it interesting to compare the populations of Hilda and Trojan asteroids. Both have a comparable capture probability in the five-planet, jumping-Jupiter model (see Nesvorný et al. 2013). Focusing on the 10 to 100 km range of sizes, the population of Trojans has a slightly steeper distribution than the Hildas: -2 versus -1.7 (e.g., Brož & Vokrouhlický 2008; Grav et al. 2011, 2012a). This can indeed be well explained by a somewhat more vigorous collisional evolution of Hildas. Note that our assumed disk source population (Figure 15 in Nesvorný & Vokrouhlický 2016) is calibrated by the Trojan statistics, and thus it has built in the steeper size distribution exponent -2 below $\simeq 100$ km size. Therefore, we naturally obtain the overabundance in the Hilda population.

3.1.5. Capture of Disk Planetesimals in the Zhongguo Population (J2/1 Resonance)

Next, we analyzed the sub-population in the stable core of the J2/1 resonance near 3.25 au (Zhongguo population). We found 57 planetesimals in our Case 1 simulation where σ_1 librates about the stable point within the J2/1 resonance. Most of these bodies occupy what is known as “island B” in the resonance (e.g., Nesvorný & Ferraz-Mello 1997; Brož & Vokrouhlický 2008; Chrenko et al. 2015). The higher eccentricity and inclination zone called “island A” is nearly empty.

This result could be considered counter-intuitive because many initial orbits of the captured particles from the trans-Neptunian disk have high eccentricities and high inclinations (see Figure 8). Note that the orbits of island A asteroids are predominantly highly inclined and have, on average, higher eccentricity compared to those in island B. However, the island A orbits also have smaller libration amplitude, thus representing a smaller phase volume than their twins in island B. Additionally, this apparent puzzle may also be solved using the findings from Ferraz-Mello et al. (1998a, 1998b), who studied the stability of objects in the J2/1 resonance. They found that during the migration of Jupiter and Saturn, the objects in island A are much more susceptible to destabilization than those in island B. When Jupiter and Saturn approached their current orbital configuration close to their mutual 5/2 mean-motion

resonance, the period and amplitude of the great inequality term in their orbits increased. Earlier phases of their orbital evolution, when the orbits of the two planets are closer to each other, have a shorter period for this mutual perturbation. At that moment, it can resonantly interact with the proper libration period in island A. Indeed, Chrenko et al. (2015) studied the orbital evolution of bodies inside the J2/1 resonance in the five-planet scenario of NM12 and confirmed this instability mechanism.

The latest census of the stable population of objects in the J2/1 resonance by Chrenko et al. (2015) indicates that there is only a handful of asteroids that are $D \simeq 10$ km. Most of them were proposed to be members of a population tail injected into the resonance from nearby C-type objects. This suggests that we can only expect of the order of unity of P/D types with these sizes. In contrast, our capture efficiency of $\simeq 6 \times 10^{-8}$, would imply about 240 of such objects in the J2/1 resonance. This mismatch is much higher than any other discussed above. We hypothesize that the survival of the J2/1 particles in our simulation is strongly enhanced by the inaccurate behavior of our secular resonances (Figure 13) and/or the missing secular forcing produced by the ice giants.

3.1.6. Capture of Disk Planetesimals in the Thule Population (J4/3 Resonance)

The most peculiar of the three first-order resonances is the J4/3. For more than a century, (279) Thule was the only known object to reside in its stable region. Only recently Brož & Vokrouhlický (2008) found two more objects located in the same zone, namely, (186024) 2001 QG207 and (185290) 2006 UB219, both $\simeq 10$ km size asteroids provided they have a low albedo of $\simeq 0.05$. We do not know if they are P/D types. Regardless, the size frequency distribution of this population is extremely odd when one considers that Thule is $D \simeq 127$ km.

In Case 1, we recorded one particle residing in the J4/3 mean-motion resonance at the end of phase 3. This confirms an enormously small capture probability at the level of $\simeq 10^{-9}$. With $\simeq 4 \times 10^9$ $D > 10$ km size disk objects, we may expect about 4 to be captured in the J4/3 resonance. Given these small numbers, our work only provides a consistency check, but it is nice that our numbers are reasonable. It is conceivable, however, that the observed small asteroids in the J4/3 resonance were from an epoch that existed before the dynamical instability or they may even be fragments from cratering events on (279) Thule. Observations of these bodies may provide us with clues we can use to deduce their zone of origin. Regardless, the existence of (279) Thule in this resonance is an enigma. It cannot easily be explained away as a captured body from the trans-Neptunian population in our model because of its large size and small capture probability.

3.1.7. Probing the Role of the Fifth Planet for Planetesimal Deposition

Finally, we make use of our fictitious Case 1 simulations where we formally set the mass of the fifth planet equal to zero (Section 2.4, also known as the “fake Case 1 simulation”). In Figure 15, we compare the cumulative semimajor axis distribution of captured planetesimals, $N(<a)$, between the full-fledged and the fake variants of the Case 1 simulation. One difference between the runs is the smaller number N_{eff} of planetesimals used in the fake variant, 200 versus 1000 million.

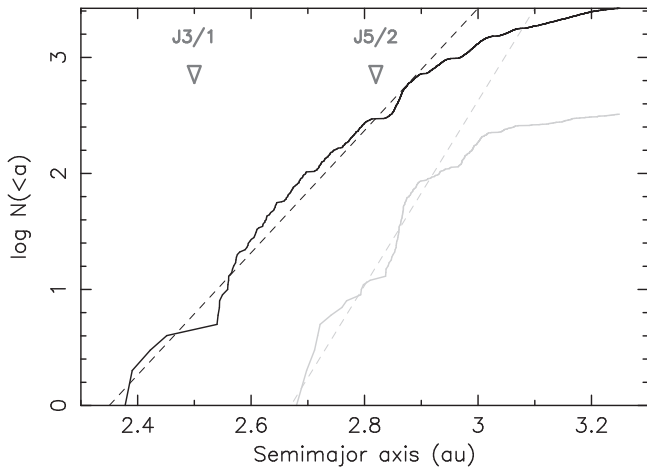


Figure 15. Cumulative distribution of semimajor axis $N(<a)$ for implanted planetesimals in the Case 1 simulation at 4 Gyr (black lines). The gray lines are for the reference simulation, where the mass of the fifth (ejected) giant planet was formally set to zero during the phase 1 and only 200 million exterior disk particles used (as opposed to one billion of particles in the full-scale simulation). The dashed lines highlight the mean linear trends of the distributions. Here we considered planetesimals below the J2/1 mean-motion resonance with Jupiter only (excluding Cybele and Hilda regions); the approximate position of the J3/1 and J5/2 resonances are indicated by triangle symbols. Orbits in these resonances are dynamically unstable on a short timescale and thus the $N(<a)$ distribution has a flat segment at their location.

Even multiplying by a factor of 5, however, we find that the $N(<a)$ of the fake variant would not reach that of the full-fledged variant. In particular, we find steeper decay of $N(<a)$ at smaller a values (dashed lines).

In quantitative terms, there are about 300 and 13 planetesimals captured below the J5/2 resonance at ≈ 2.82 au in the full-fledged and fake simulation, respectively. Here, the population ratio is nearly a factor of 30. We believe that this difference is due to the missing gravitational effects of the fifth giant planet. Moreover, the full-fledged simulation places some objects below the J3/1 resonance at 2.5 au. We conclude from this that the effects of the fifth planet are crucial to reproducing the constraints provided by P/D-type asteroids.

Note that indirect effects are present here because Jupiter’s orbit does not evolve exactly the same way in the two simulations. Still, the lowest semimajor axis value of the captured objects in the latter simulation was about 2.68 au, which is comparable to the results in Levison et al. (2009). This may seem odd because we used about six times more particles than Levison et al. (2009), 200 versus 31 million. The orbital evolution of Jupiter in the two simulations, however, is radically different; this likely explains the difference.

3.2. Case 2

We now continue by examining the Case 2 simulation results. Figure 16 shows the distribution of the osculating orbital elements of planetesimals at the beginning of phase 2. The overall characteristics are essentially the same as for Case 1 in Figure 8, although there is one significant difference. There is an overabundance of particles along the aphelion line $Q \approx 3.55$ au (dashed gray line at the top panel). According to Figure 7, we observe that this is about the smallest semimajor axis value that was temporarily attained by the fifth planet during the planetary instability phase. As the fifth planet was performing small jumps in and out around this value, it

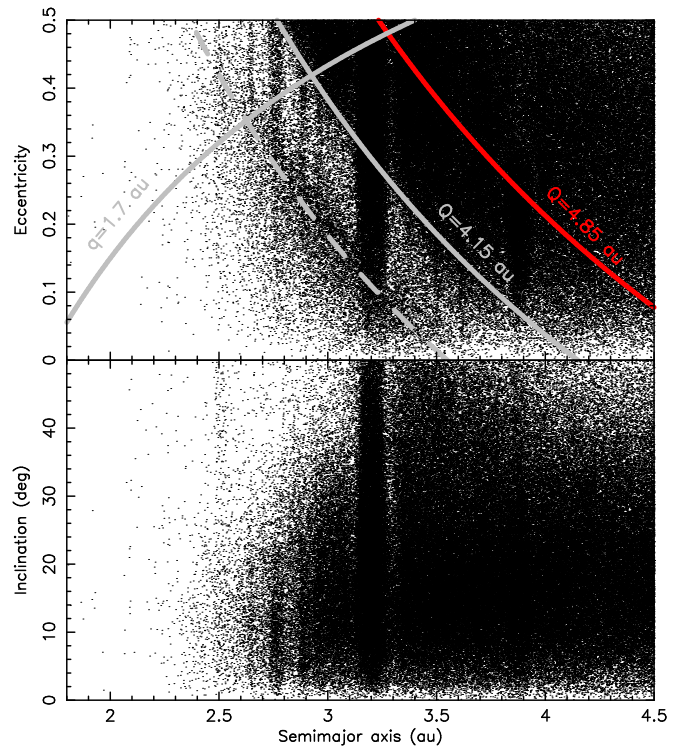


Figure 16. Osculating orbital elements, semimajor axis vs. eccentricity (top) and semimajor axis vs. inclination (bottom), of particles selected to continue at the beginning of the phase 2 of our Case 2 simulation. About half of the particles reside in the powerful, low-order mean-motion resonances with Jupiter (such as J3/1, J2/1 or J3/2), while the remaining population was scattered onto orbits partially overlapping with the main-belt zone. Many of them that have aphelion larger than ≈ 4.85 au indicated by the red line will be swiftly eliminated in the phase 2 by close encounters with Jupiter. A denser concentration of particles continues to aphelion distance ≈ 4.15 au (gray curve at the top), which is roughly correlated with the range of semimajor axis values attained by the fifth planet (Figure 7). The deepest brief jumps of the fifth planet led to its semimajor axis value between $\approx (3.5\text{--}3.6)$ au. This correlates with over-density of particles with aphelia in this range (see the dashed gray line for $Q = 3.55$ au). Orbits with perihelii smaller than ≈ 1.7 au (gray curve at the top) would be eliminated by close encounters with terrestrial planets, and they are eliminated during our phase 3.

efficiently stirred the planetesimal population and captured them onto random orbits from resonance locations with Jupiter. The longer timespan of this critical part of the planetary instability also implies that more test disk planetesimals were captured onto orbits in the main belt region than in the Case 1 simulation—see Table 1.

While this planetary behavior increases the efficiency of planetesimal capture, the fifth planet’s deeper visits into the heliocentric zone are also responsible for producing excessive excitation of the in situ asteroid population (Roig & Nesvorný 2015). On the other hand, we verified that the terrestrial planet system, including Mars, were left on reasonable orbits. Therefore, while one should not regard the Case 2 simulation as fully realistic, it is still useful to consider our results as an approximate upper bound on the test disk planetesimal-capture efficiency.

Figure 17 shows how the Case 2 simulated population undergoes decay during phases 2 and 3. Apart from more particles in the simulation, the basic features are the same as Case 1. Finally, Figure 18 shows osculating orbits of 9603 planetesimals captured in the sub-Jupiter zone in the Case 2 simulation (right panels) compared to the observed asteroids

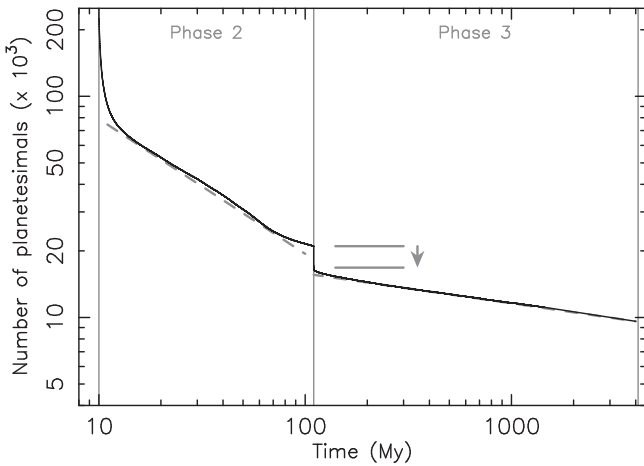


Figure 17. Number of particles remaining in the Case 2 simulation through the phases 2 and 3 (solid line). Each of the two phases shows transient phenomena at the beginning: (i) many particles have been left on very unstable orbits at the beginning of the phase 2 (Figure 12) and these were swiftly scattered by Jupiter, and (ii) orbits with $q < 1.5$ au and $Q > 15$ au were instantly removed at the beginning of the phase 3 by our tightened elimination criteria, producing a drop in the population number. The dashed lines are power-law approximations $N \propto t^{-\alpha}$ with exponents $\alpha \simeq 0.62$ in the phase 2 and $\alpha \simeq 0.14$ in the phase 3.

(left panels). For reference, a factor of 2 more planetesimals were captured in Case 2 than Case 1 (9603 versus 4610), however, the overall features are the same as in the Case 1 simulation.

In what follows, we briefly comment on how the results of the two simulations differ. The population of planetesimals captured in the inner main belt is substantially larger now, containing 37 bodies, compared to 5 for Case 1. This is an increase of $\simeq 7.4$. Many are piled up near the J3/1 resonance, with semimajor axes > 2.4 au, but some orbits now reach 2.3 au. We also find that one planetesimal was captured into the Phocaea region of the main belt (i.e., high-inclination main belt orbits with $2.2 < a < 2.5$ au). The central and outer main belt zone between the J3/1 and J2/1 resonances contains $\simeq 2.5$ times more planetesimals than in Case 1 (7009 versus 2665 test disk planetesimals). The overall increase in numbers is a consequence of the increase in the population in low- Q orbits from Figure 16. The number of planetesimals captured onto more distant orbits in the Cybele population is comparable to the Case 1 simulation. We again see the anomalous sub-population of Kozai librators with high eccentricities and inclinations (roughly 242 bodies).

Populations captured in first-order resonances are also comparable to the Case 1 situation, with only slightly more objects librating in the J2/1 resonance. As suspected above, however, the fact that we are missing low secular frequencies and other mismatched details of planet migration may imply that our captured populations are perhaps larger than they should have been. The most robust population captured in the J3/2 resonance, the Hilda region, is comparable to the Case 1 simulation. We now record two bodies captured in the J4/3 resonance, the Thule population, rather than the one we had before.

Finally, Figure 19 shows comparison of the cumulative distribution of semimajor axes for captured test disk planetesimals $N(<a)$ in both the full-fledged Case 2 simulation and the fake variant with a zero mass of the fifth planet (compare with Figure 15). Apart from the larger capture efficiency as

compared to the Case 1 simulation, the results are comparable. The smallest semimajor axis value reached in the fake variant is now $\simeq 2.6$ au. This lower value is due to the different history that Jupiter makes when it is undergoing jumps in semimajor axis. The ratio of objects below the J5/2 ($\simeq 2.82$ au) in both variants is again $\simeq 30$, which is far more than the factor of 5 in number N_{eff} of planetesimals in both simulations. This again supports the importance of direct stirring produced by the fifth planet for test disk planetesimal deposition onto heliocentric orbits in the innermost parts of the main belt.

4. DISCUSSION

4.1. Population Trends of Captured Disk Planetesimals

Disk planetesimals captured in our simulations happen to populate all zones of stability where P/D-type asteroids are observed. For the first time, we have a model that can inject planetesimals into the inner main belt. An increasing number of bodies are implanted into more distant zones of the belt and in the first-order mean-motion resonances with Jupiter. This steady increase as we move outward in heliocentric distance is a reflection of not only the closer proximity to the giant planet region during the instability period, and the source of the ejected disk planetesimals, but also the larger available phase-space volume of orbital regions that are currently stable.

We find that planetesimal capture is essentially a chaotic process, dominated by resonance transport combined with (i) indirect deposition produced by giant planets undergoing small-scale jumps in semimajor axis due to mutual encounters, and (ii) direct deposition from encounters between ejected disk planetesimals and a fifth giant planet roaming the sub-Jupiter heliocentric zone. Moreover, we believe that the relative proportion of captured planetesimals in our simulations is roughly correct because the currently observed asteroid populations fill all of the available zones of orbital stability.

The successes of the Case 1 model include the following.

1. The final orbits of the giant planets, and the relative proportion of the captured sub-populations, are grossly correct.
2. We match reasonably well the estimated number and sizes of the largest P/D bodies in (i) the central/outer main belt, (ii) those bodies combined with the the Cybele region, and (iii) the Hilda population (within uncertainty).
3. The same model was able to reproduce the Jupiter Trojan population and the starting conditions expected for irregular satellite populations of the giant planets (Nesvorný et al. 2013, 2014a). For the latter, collisional grinding of the captured populations do an excellent job of reproducing the observed irregular satellite size frequency distributions (Bottke et al. 2013).
4. The same model can reproduce the key components of the trans-Neptunian populations that were implanted from the same source zone, namely, a massive primordial disk of planetesimals between 23 and 30 au (i.e., the dynamically hot classical disk and the resonant populations; Nesvorný 2015a, 2015b; Nesvorný & Vokrouhlický 2016).

The failures of the Case 1 model include the following.

1. We under-predict the absolute numbers of $D > 30$ km P/D types in the inner main belt by a factor of ~ 3 or so.

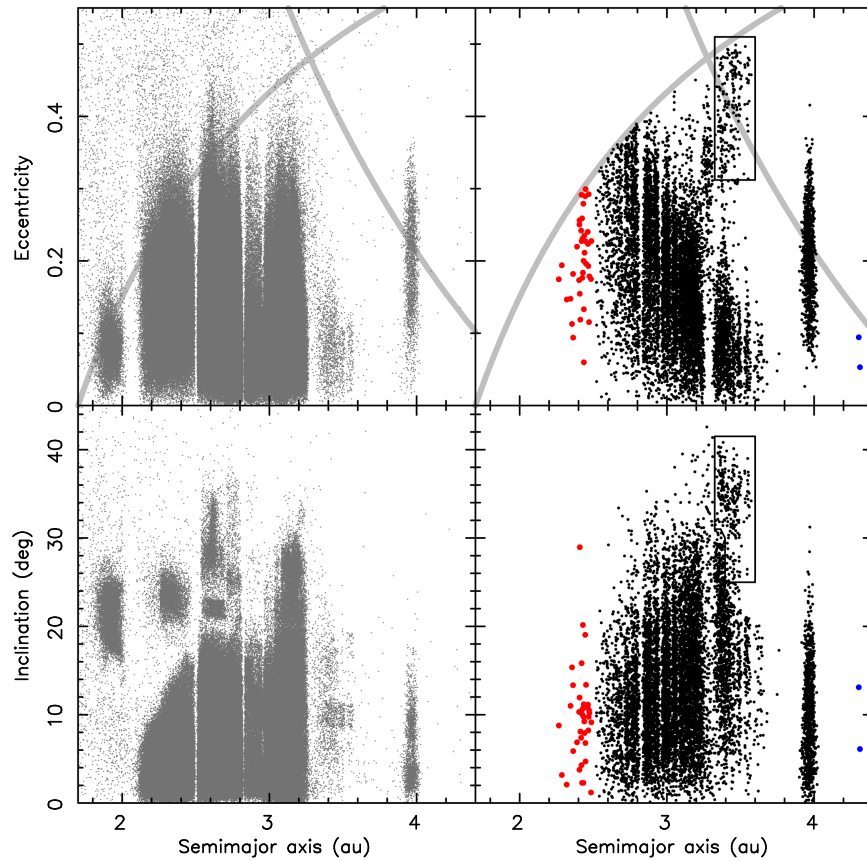


Figure 18. Particles in the main-belt, Hilda, and Thule orbital zones that remained in the Case 2 simulation at 4 Gyr (right column) compared with the observed population of asteroids (left column; see also Figure 1). Top panels show semimajor axis vs. eccentricity (gray lines as in Figure 1), bottom panels show semimajor axis vs. inclination. The red symbols highlight particles interior to the J3/1 mean-motion resonance with Jupiter. The blue symbols represent two particles resident in the stable zone of J4/3 mean-motion resonance with Jupiter. The rectangle/polygon in the right panels indicate population of particles captured in Kozai states in our simulation (see discussion in the main text).

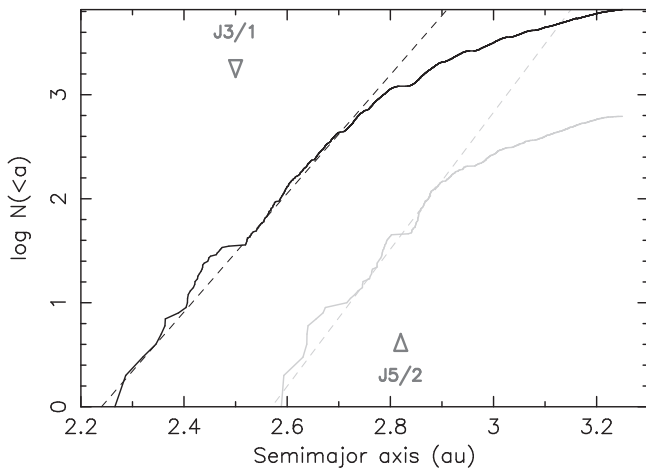


Figure 19. Cumulative distribution of semimajor axis $N(<a)$ for implanted planetesimals in the Case 2 simulation at 4 Gyr (black lines). The gray lines are for the reference simulation, where the mass of the fifth (ejected) giant planet was formally set to zero during the phase 1 and only 200 million exterior disk particles used (as opposed to one billion of particles in the full-scale simulation). The dashed lines highlight the mean linear trends of the distributions. Here we considered planetesimals below the J2/1 mean-motion resonance with Jupiter only (excluding Cybele and Hilda regions); the approximate position of the J3/1 and J5/2 resonances are indicated by triangle symbols. Orbits in these resonances are dynamically unstable on a short timescale and thus the $N(<a)$ distribution has a flat segment at their location.

2. We over-predict the absolute numbers of $D > 10$ km P/D types across various main belt regions by a factor of ~ 10 or so.
3. We over-predict the absolute numbers of $D > 10$ km P/D types in the Hilda region by a factor of $\sim 3-4$ or so.
4. We do not reproduce all aspects of the Zhongguo (J2/1) population.
5. We predict some bodies in Kozai resonance in the outer main belt that have yet to be observed.

It is possible some minor mismatch issues between model and observations for large P/D-type asteroids could be solved by modifying our estimate of the size frequency distribution of disk planetesimals located exterior to giant planets between ≈ 23 and 30 au by a factor of 2 or so in places. There is a limit to how far we can go, however, because fixing a problem for one model component may open up problems for another component. In fact, one of the strengths of our work is that our chosen disk planetesimal size distribution, scaled from that found in the Jupiter Trojan population, works so well everywhere. Moreover, we also find that its shape is also very consistent with the predicted projectile size frequency distribution that struck Pluto, as determined by the crater size frequency distribution identified by images from the New Horizons mission (Singer et al. 2015).

If these minor changes are incapable of correcting the over-prediction of P/D types in the main belt, then a second

possibility is that additional five-planet-instability model realizations are needed. Consider the trends between Cases 1 and 2. In Case 1, there were 5, 2665, and 1214 test planetesimals injected into the main belt between 2.1–2.5 au, 2.5–3.25 au, and 3.25–3.6 au, respectively, while for Case 2, it was 37, 7009, and 1505, respectively (Table 1). The ratios of Case 2 values to Case 1 are 7.4, 2.6, and 1.2, respectively. The reason for this difference is that disk planetesimals were possibly captured into the main belt region via gravitational interactions with a fifth giant planet encountering Jupiter, and the fifth planet in Case 2 spends more time with sub-Jupiter perihelion values than in Case 1 (Figures 4 and 6). Intriguingly, the biggest difference is seen for the inner main belt, while the number captured in the Cybele region is virtually the same. The inner main belt is also where Case 1 under-predicts the observed P/D types with $D > 30$ km by a factor of 3 or so.

Accordingly, we believe a new model realization where the fifth planet spends more time with sub-Jupiter perihelion values than Case 1 but less than Case 2 would satisfy our under-prediction of P/D-types for the inner main belt while only modestly influencing the good fits in the central/outer main belt and Hilda regions. This putative “Case 1.5” run needs to avoid the more problematic issues with Case 2; recall that Case 2 is a failure because it dynamically excites the main belt too much to match observations (Roig & Nesvorný 2015). We see no reason why this proposed “Case 1.5” realization, which is fairly similar to Case 1 in most respects, would not work.

The inability of the model to correctly fill stable niches like the Zhongguos likely depends on the precise details of how the real giant planets migrated to their final orbits. Our model does not exactly reproduce the orbits of Jupiter and Saturn, and for computational expediency, we have not included Uranus and Neptune in the late phases of our model runs. Moreover, the zone of stability for the J2/1 resonance is small, and our model is missing the secular resonances induced by those giant planets left out of our simulation. We suspect that these problems will eventually be solved by higher resolution and small changes to our initial model conditions. Similarly, we suspect that the small population located adjacent to the J2/1 resonance that appears to be stuck in a Kozai state is also an artifact of imperfect final giant planet orbits.

The biggest model failure discussed above concerns our model mismatch with the smaller P/D-type asteroids. We discuss possible solutions in the section below.

4.2. Survival of P/D Types in the Main Belt over 4 Billion Years

We see several ways to account for this apparent overabundance of $D > 10$ km P/D-type asteroids, all of which may contribute in some fashion.

Collision Evolution. Levison et al. (2009) was the first to suggest that the mismatch between the number of captured planetesimals and their currently observed population was that the implanted bodies experienced substantial collisional grinding over 4 Gyr (see also Bottke et al. 2015).⁸ They assumed that the captured P/D types, which are likely to be highly porous, low-density bodies analogous to CI/CM carbonaceous chondrites, disrupted more easily than S-type

main asteroids, and some may be analogous to ordinary chondrites. By choosing a weaker effective strength against collisions for the captured bodies, Levison et al. (2009) was able to meet the constraints. Interestingly, though, calculations by Jutzi et al. (2015) suggest that P/D types may have higher strengths against collisions than expected, which in turn would lead to less grinding. Given that our Case 1 simulations have a smaller overabundance of P/D types than found in Levison et al. (2009), we suspect that we may be able to match constraints with the new parameters. We leave this interesting problem for future work.

Thermal Destruction En Route to the Inner Solar System. A portion of the disk planetesimal population could also have been eliminated by thermal destruction. As ejected disk planetesimals move closer to the Sun, some would be destroyed by the sudden escape of volatiles. This is a well-known phenomenon; many comets have been seen to disrupt en route to orbits closer to the Sun (e.g., 57P/du Toit–Neujmin–Delporte or 73P/Schwassmann–Wachmann 3). In fact, this mechanism has been proposed to solve the so-called “fading problem” among nearly isotropic comets (i.e., orbital evolution models of new, nearly isotropic comets consistently predict far more returning comets that are observed; Levison et al. 2002). This was also the solution suggested by Brož et al. (2013), who studied the statistics of medium- to large-size asteroid families potentially affected by comet bombardment during the Nice model (see also Levison et al. 2002). Among the most ancient families, they found a deficit of medium-size families relative to large families. They hypothesized that the corresponding projectile flux during the late heavy bombardment period was lower because of some of the bodies disrupted as they approached the Sun. Finally, this destruction mechanism seems to be important for low-albedo, near-Earth asteroids (Granvik et al. 2016). The main unknown in invoking this mechanism is the putative efficiency of disruption among $D > 10$ km comets.

Yarkovsky-effect-driven Depletion. Some additional dynamical depletion mechanisms come into play for smaller heliocentric distances. Note that in phase 3, we already account for how some bodies may escape via weak gravitational resonances over 4 Gyr. We left out, however, the gravitational effects of the terrestrial planets, some of which may produce diffusive resonances (e.g., Mars). A more important mechanism, though, is the non-gravitational (thermal) forces known as the Yarkovsky effect (e.g., Bottke et al. 2006; Vokrouhlický et al. 2015). The Yarkovsky effect allows $D < 30$ km asteroids to drift inward toward or outward away from the Sun via the absorption of sunlight and the anisotropic re-radiation of this energy away as infrared photons. This may also cause some asteroids to reach resonances that take them out of the main belt zone.

Here, we illustrate the potential of the dynamical losses via the Yarkovsky effect in the case of the inner main-belt D-type asteroids identified by DeMeo et al. (2014). Consider asteroid (15112) Arlenewolfe, which has the smallest value of semimajor axis ($a \simeq 2.3$ au) from this sample. The information about the physical parameters of this body is scanty, with only a size estimate of $\simeq 7.4$ km and geometric albedo of $\simeq 0.07$ from *WISE* observations (e.g., Masiero et al. 2011). Nothing is known about its rotation state. We assume it has a low bulk density of $1\text{--}1.3$ g cm⁻³, which is in the right ballpark for the related C-complex asteroids, but also has been determined from observations of binary systems among Jupiter Trojans (e.g.,

⁸ Actually, the over-prediction factor in Levison et al. (2009) was even larger than in our paper, some ~ 50 to ~ 100 , perhaps due to a combination of a larger assumed source population and more efficient estimated capture probabilities.

Marchis et al. 2006, 2014; even smaller density value is not impossible, see Mann et al. 2007). This value is conservative also because many comets, the first cousins to the P/D types discussed here, have bulk densities between 0.3 and 0.7 g cm⁻³ (e.g., Weissman et al. 2004). We find that (15112) Arlenewolfe could have accumulated a maximum change in semimajor axis of $\simeq 0.3$ au over 4 Gyr, provided that the obliquity remained near 0° or 180°. If captured onto an orbit just inside the J3/1 resonance at 2.5 au, like those test disk planetesimals in our simulations, it could have easily drifted to its current orbit. Alternatively, a fictitious twin of this body drifting outward rather than inward could have been readily lost via the J3/1 resonance many Gyrs ago.

We expect the small-body P/D-population to drop by a factor of two or more over long timescales as they drift into nearby resonances and are driven into the planet-crossing region. Thus, Arlenewolfe-size bodies that can potentially drift as far as $\simeq 0.3$ au over 4 Gyr could lose much larger fractions of their initial population. For all of these reasons, the currently observed population of smaller P/D-type asteroids in the main belt may represent a lower limit for the population captured into the main belt 4 Gyr ago.

Dynamical depletion by the Yarkovsky effect becomes smaller at larger heliocentric distance, namely, in the outer main belt, the Cybele zone, and especially in the resonant populations like the Hildas (where it only contributes a small component to the eccentricity diffusion; e.g., Brož & Vokrouhlický 2008). Interestingly, the mismatch between the estimate of the captured population of planetesimals and the observed population of dark asteroids is least among the Hilda objects (Section 3.1), possibly due to the negligible dynamical depletion.

4.3. Was Ceres Captured from the Primordial Disk?

An intriguing possibility raised by McKinnon (2008, 2012) is that (1) Ceres, the largest main belt asteroid, might be a captured planetesimal from the primordial disk originally located beyond. McKinnon (2008, 2012) made his case based on insights from the Nice model (e.g., Levison et al. 2009) and the fact that many of Ceres' characteristics, namely, its large size ($\simeq 945$ km), differentiated nature, low bulk density, and estimated composition, all share similarities with known KBOs. This hypothesis was potentially strengthened recently by the confirmation of ammoniated phyllosilicates of the surface of Ceres (De Sanctis et al. 2015). The presence of these materials could mean that Ceres formed far beyond the snowline, where ammonia is readily found, or that outer solar system materials migrated inward and were accreted onto Ceres.

Here, we estimate the probability of a Ceres capture using Case 1 results. Our computations indicate that the primordial disk beyond Neptune between $\simeq 23$ and 30 au may have once had 3600–14,000 Ceres-sized bodies. If we use the capture probability of disk planetesimals pertaining to the outer main belt and Cybele region, $\simeq 3.9 \times 10^{-6}$ per test disk planetesimal, then the capture probability of Ceres is 1%–6%. Ceres, however, is located at 2.77 au, which is closer to the Sun than the J5/2 resonance at $\simeq 2.82$ au. This lowers the capture probability per disk planetesimal to $\simeq 3 \times 10^{-7}$, such that the capture probability of Ceres is 0.1%–0.4%. This value is low

enough that we do not favor it as an explanation for the origin of Ceres.

This does not mean, however, that Ceres cannot be an ejected planetesimal from the zone of the giant planets. Recent planet formation models show that there are dynamical ways to deliver planetesimals from the giant planet zone very early in Solar System history (e.g., Walsh et al. 2011; Levison et al. 2015). It could be that Ceres is from this region rather than the much more distant primordial disk.

Regardless, the reader should keep in mind that given Ceres' very large size, it is statistically unlikely for it to be captured without also implanting much of the main belt's C-complex asteroid population at the same time. Future work will be needed to see whether models associated with the planet formation/solar nebular era can realistically deliver Ceres from beyond the snowline while also matching the associated main belt constraints.

4.4. The Tagish Lake Meteorite: A Plausible Sample from a Primordial Kuiper Belt Object

It is interesting to note also that there is a fraction of D-type candidate asteroids in the Mars-crossing and near-Earth object (NEO) populations (e.g., Carry et al. 2016). According to Carry et al., D-types with $D < 5$ km originating from the innermost parts of the main belt are only about twice as less populous than those originating from the outer main belt. We do not expect many D-types from the outer main belt to be long-lived members of the NEO population; outer main belt sources of NEOs are only expected to make up about 10%–15% of the overall population, with most having $a > 2.5$ au (e.g., Bottke et al. 2002). Therefore, these observations imply that we need a prominent source of D-types in the inner main belt that still exists today. We argue that the most likely source of D-types in the inner main belt is the captured disk planetesimals described by our model.

Along these lines, it is interesting to consider the singular meteorite known as Tagish Lake (e.g., Brown et al. 2002; Hildebrand et al. 2006). This primitive C2-type carbonaceous chondrite was recovered almost immediately after falling onto a frozen Canadian lake after its parent bolide disrupted high in the atmosphere on 2000 January 18. While similar to CM and CI meteorites in some ways, it is also distinct from them as well in many of its geochemical properties (e.g., Vernazza et al. 2013).

Tagish Lake has spectral properties that resemble X-, T-, and less red D-type asteroids (Hiroi et al. 2001; Vernazza et al. 2013). For example, Vernazza et al. (2013) found that Tagish Lake has spectral and reflectance properties similar to the D-type main belt asteroid (368) Haidea, located at $a \simeq 3.07$ au. Its spectra also match those of carbonaceous interplanetary dust particles, or IDPs; these bodies previously had no match in worldwide meteorite collections (e.g., Bradley et al. 1996; Hildebrand et al. 2006). Note that the most likely source of these IDPs are disrupted JFCs, and their source population that was also derived from the primordial disk (e.g., Nesvorný et al. 2010). Conversely, Tagish Lake spectra are inconsistent with the spectral properties and reflectance of Ch- and Cgh-type asteroids, which are the likely source of CM chondrites. Vernazza et al. (2013) used this information to argue that Tagish Lake formed further away from the Sun than the CM parent bodies.

The (a, e, I) orbit of the Tagish Lake bolide, according to a recent revision reported in Brown et al. (2016), was (1.98 au, $0^\circ.55$, and 2°), respectively. Using the Bottke et al. (2002) NEO model, we find that this body most likely came from the ν_6 secular resonance or the intermediate source Mars-crossing region, which are both inner main belt sources. Similarly, using the updated NEO model provided by Granvik et al. (2016), it has an 82% chance of coming from the ν_6 resonance, an 11% chance of coming from the J3/1 resonance, and a 6.5% chance of coming from the Hungaria asteroid region. The highest probabilities here suggest that Tagish Lake's immediate precursor came from the inner main belt.

It is possible that the Tagish Lake meteorite is a fragment from a JFC that was decoupled from the gravitational clutches of Jupiter (e.g., Levison et al. 2006). Simulations from Levison et al. (2006), however, suggest that this is an unlikely circumstance; the (a, e) orbit of the Tagish Lake bolide is just outside where we would expect a decoupled JFC to be found.

Using the clues provided above, and making reasonable inferences, we argue that the Tagish Lake meteorite is probably a sample from a D-type asteroid in the inner main belt. Note that we cannot rule out other possibilities, but they are less likely based on the available information. This conclusion fits well with the observation of D-types in the inner main belt and Mars-crossing population (DeMeo et al. 2015; Carry et al. 2016). Thus, given the work presented in this paper, we predict that the Tagish Lake parent body was a captured member of the primordial disk population of comet-like objects that used to exist beyond the orbit of Neptune. This means the properties of the Tagish Lake meteorite may allow us to investigate the composition and nature of those planetesimals that formed at great distances from the Sun.

5. CONCLUSIONS

Here, we briefly summarize the main results of our paper. We assumed here that our Solar System once had five giant planets locked in a stable configuration between 5 and 22 au: Jupiter, Saturn, Uranus, Neptune, and an extra Neptune-like body. Beyond these worlds existed a massive disk of comet-like planetesimals between 23 and 30 au containing possibly thousands of Pluto-sized bodies, ≈ 50 million $D > 100$ km bodies, and a host of smaller bodies. This system eventually experienced a dynamical instability, which led to a wide range of effects: the planets migrated and encountered one another, the disk was dispersed, and disk planetesimals were sent into the giant planet realm where they could interact with the gas giants. Eventually, the extra Neptune-sized body was ejected out of the Solar System via an encounter with Jupiter, but not before it injected numerous disk planetesimals into stable niches throughout the Solar System.

Here, we studied how interactions between the putative fifth giant planet, the remaining giant planets, and disk planetesimals allowed some disk planetesimals to be captured in the inner, central, and outer main regions, as well as Cybele and the resonant Hilda and Thule regions. We deduced the size of the populations in each zone and compared them to the known populations of P/D-type asteroids found there.

Overall, we found a high degree of success, with reasonable matches within uncertainties found between our model and observations of the largest known P/D-type asteroids. We confirmed the main conclusions of Levison et al. (2009), but

our model was more successful at obtaining the correct details of the captured population. For example, we reproduced, for the first time, the D-type asteroid population seen in the inner main belt ($a < 2.5$ au). Our match to $D > 10$ km P/D-types in the main belt was less successful, with our model overestimating observations by a factor of ~ 10 . We argue that this is because the P/D-types have experienced substantial attrition over time. Likely removal mechanisms include disruption of disk planetesimals en route to the inner solar system, main belt collision evolution over 4 Gyr, and dynamical removal over 4 Gyr via Yarkovsky thermal forces/resonances. That said, we admit that a detailed comparison of the captured planetesimals distribution across the main belt with the observed population of D- and P-type objects is beyond the scope of this paper. It will be an excellent project for a follow-up work.

The broad fidelity of our model results provide powerful evidence that (i) our Solar System experienced an early instability, (ii) the giant planets encountered one another and dispersed a massive planetesimal disk, and (iii) that Jupiter ejected a Neptune-like body during the endgame of the instability that briefly interacted with the asteroid belt. Moreover, it leads us to predict that most P/D-type asteroids found across the main belt, among the Mars-crossing population, and in the NEO population are actually surviving remnants of this primordial disk population. The observed spectral and albedo differences that correlate with heliocentric distance may result from yet unknown alteration processes (see, e.g., Fitzsimmons et al. 1994; Carvano et al. 2003).

Accordingly, we argue that sample return missions to highly accessible D-type NEOs are effectively missions to the evolved Kuiper Belt objects (e.g., Carry et al. 2016). Likewise, we predict that the Tagish Lake meteorite is a sample from a D-type asteroid that was residing in the inner main belt. We believe that it represents material from a source population that now comprises the Kuiper Belt.

We thank an anonymous referee for suggestions that helped to improve the paper. The work of David Vokrouhlický was supported by the Czech Grant Agency (grant GA13-01308S). Research funds for William Bottke were provided by NASA's OSIRIS-REx mission (NASA Contract NNM10AA11C; D. S. Lauretta, PI) and NASA's Solar System Evolution Research Virtual Institute (SSERVI) program through a grant to the Institute for the Science of Exploration Targets (NNA14AB03A), at the Southwest Research Institute in Boulder. Resources supporting this work were provided by the NASA High-End Computing (HEC) Program through the NASA Advanced Supercomputing (NAS) Division at Ames Research Center.

REFERENCES

- Batygin, K., Brown, M. E., & Betts, H. 2012, *ApJL*, **744**, L3
 Bottke, W. F., Brož, M., O'Brien, D. P., et al. 2015, in *Asteroids IV*, ed. P. Michel et al. (Tucson, AZ: Univ. Arizona Press), 701
 Bottke, W. F., Morbidelli, A., Jedicke, R., et al. 2002, *Icar*, **156**, 399
 Bottke, W. F., Vokrouhlický, D., Minton, D., et al. 2012, *Natur*, **485**, 78
 Bottke, W. F., Vokrouhlický, D., Nesvorný, D., & Moore, J. 2013, *Icar*, **223**, 775
 Bottke, W. F., Vokrouhlický, D., Rubincam, D. P., & Nesvorný, D. 2006, *AREPS*, **34**, 157
 Bradley, J. P., Keller, L. P., Brownlee, D. E., & Thomas, K. L. 1996, *M&PS*, **31**, 394
 Brassier, R., & Lee, M.-H. 2015, *AJ*, **150**, 157

- Brasser, R., Morbidelli, A., Gomes, R., Tsiganis, K., & Levison, H. F. 2009, *A&A*, **507**, 1053
- Brown, P. G., Revelle, D. O., Tagliaferri, E., & Hildebrand, A. R. 2002, *M&PS*, **37**, 661
- Brown, P. G., Wiegert, P., Clark, D., & Tagliaferri, E. 2016, *Icar*, **266**, 96
- Brož, M., Morbidelli, A., Bottke, W. F., et al. 2013, *A&A*, **551**, A117
- Brož, M., & Vokrouhlický, D. 2008, *MNRAS*, **390**, 715
- Brož, M., Vokrouhlický, D., Morbidelli, A., Bottke, W. F., & Nesvorný, D. 2011, *MNRAS*, **414**, 2716
- Carry, B., Solano, E., Eggl, S., & DeMeo, F. E. 2016, *Icar*, **268**, 340
- Carvano, J. M., Mothé-Diniz, T., & Lazzaro, D. 2003, *Icar*, **161**, 356
- Chrenko, O., Brož, M., Nesvorný, D., Tsiganis, K., & Skoulidou, D. K. 2015, *MNRAS*, **451**, 2399
- Cloutier, R., Tamayo, D., & Valencia, D. 2015, *ApJ*, **813**, 8
- Deienno, R., Nesvorný, D., Vokrouhlický, D., & Yokoyama, T. 2014, *AJ*, **148**, 25
- DeMeo, F. E., Alexander, C. M. O'D., Walsh, K. J., Chapman, C. R., & Binzel, R. P. 2015, in *Asteroids IV*, ed. P. Michel et al. (Tucson, AZ: Univ. Arizona Press), 13
- DeMeo, F. E., Binzel, R. P., Carry, B., Polishook, D., & Moskovitz, N. A. 2014, *Icar*, **229**, 392
- DeMeo, F. E., & Carry, B. 2014, *Natur*, **505**, 629
- De Sanctis, M. C., Ammannito, E., Raponi, A., et al. 2015, *Natur*, **528**, 241
- Durda, D. D., Bottke, W. F., Nesvorný, D., et al. 2007, *Icar*, **186**, 498
- Emery, J. P., Marzari, F., Morbidelli, A., French, L. M., & Grav, T. 2015, in *Asteroids IV*, ed. P. Michel et al. (Tucson, AZ: Univ. Arizona Press), 203
- Ferraz-Mello, S., Michtchenko, T. A., Nesvorný, D., Roig, F., & Simula, A. 1998a, *P&SS*, **46**, 1425
- Ferraz-Mello, S., Michtchenko, T. A., & Roig, F. 1998b, *AJ*, **116**, 1491
- Fitzsimmons, A., Dahlgren, M., Lagerkvist, C.-I., Magnusson, P., & Williams, I. P. 1994, *A&A*, **282**, 634
- Franklin, F., Lewis, N. K., Soper, P. R., & Holman, M. J. 2004, *AJ*, **128**, 1391
- Granvik, M., Morbidelli, A., Jedicke, R., et al. 2016, *Natur*, **530**, 303
- Grav, T., Mainzer, A. K., Bauer, J., et al. 2011, *ApJ*, **742**, 40
- Grav, T., Mainzer, A. K., Bauer, J., et al. 2012a, *ApJ*, **744**, 197
- Grav, T., Mainzer, A. K., Bauer, J. M., Masiero, J. R., & Nugent, C. R. 2012b, *ApJ*, **759**, 49
- Hahn, J. M., & Malhotra, R. 1999, *AJ*, **117**, 3041
- Hildebrand, A. R., McCausland, P. J. A., Brown, P. G., et al. 2006, *M&PS*, **41**, 407
- Hiroi, T., Zolensky, M. E., & Pieters, C. M. 2001, *Sci*, **293**, 2234
- Holman, M. J., & Murray, N. W. 1996, *AJ*, **112**, 1278
- Jewitt, D., & Haghighipour, N. 2007, *ARA&A*, **45**, 261
- Jutzi, M., Holsapple, K., Wünneman, K., & Michel, P. 2015, in *Asteroids IV*, ed. P. Michel et al. (Tucson, AZ: Univ. Arizona Press), 679
- Kasuga, T., Usui, F., Hasegawa, S., et al. 2012, *AJ*, **143**, 141
- Knežević, Z., Lemaître, A., & Milani, A. 2002, in *Asteroids III*, ed. W. F. Bottke et al. (Tucson, AZ: Univ. Arizona Press), 603
- Knežević, Z., Milani, A., Farinella, P., Froeschle, Ch., & Froeschle, Cl. 1991, *Icar*, **93**, 316
- Kozai, Y. 1962, *AJ*, **67**, 591
- Lagerkvist, C.-I., Fitzsimmons, A., Magnusson, P., & Williams, I. P. 1993, *MNRAS*, **260**, 679
- Levison, H. F., Bottke, W. F., Gounelle, M., et al. 2009, *Natur*, **460**, 364
- Levison, H. F., Kretke, K. A., & Duncan, M. J. 2015, *Natur*, **524**, 322
- Levison, H. F., Morbidelli, A., Dones, L., et al. 2002, *Sci*, **296**, 2212
- Levison, H. F., Morbidelli, A., Tsiganis, K., Nesvorný, D., & Gomes, R. 2011, *AJ*, **142**, 152
- Levison, H. F., Terrell, D., Wiegert, P. A., Dones, L., & Duncan, M. J. 2006, *Icar*, **182**, 161
- Liou, J.-C., & Malhotra, R. 1997, *Sci*, **275**, 375
- Malhotra, R. 1995, *AJ*, **110**, 420
- Mann, R. K., Jewitt, D., & Lacerda, P. 2007, *AJ*, **134**, 1133
- Marchis, F., Durech, J., Castillo-Rogez, J., et al. 2014, *ApJL*, **783**, L37
- Marchis, F., Hestroffer, D., Descamps, P., et al. 2006, *Natur*, **439**, 565
- Masiero, J. R., Mainzer, A. K., Grav, T., et al. 2011, *ApJ*, **741**, 68
- Masset, F., & Snellgrove, M. 2001, *MNRAS*, **320**, L55
- Matter, A., Guillot, T., & Morbidelli, A. 2009, *P&SS*, **57**, 816
- McKinnon, W. B. 2008, *ACM*, **1405**, 8389
- McKinnon, W. B. 2012, *ACM*, **1667**, 6475
- Milani, A., & Nobili, A. M. 1985, *A&A*, **144**, 261
- Minton, D. A., & Malhotra, R. 2009, *Natur*, **457**, 1109
- Minton, D. A., & Malhotra, R. 2011, *ApJ*, **732**, 53
- Morbidelli, A. 2002, *Modern Celestial Mechanics* (London, New York: Taylor and Francis)
- Morbidelli, A., Brasser, R., Gomes, R., Levison, H. F., & Tsiganis, K. 2010, *AJ*, **140**, 1391
- Morbidelli, A., & Crida, A. 2007, *Icar*, **191**, 158
- Morbidelli, A., & Nesvorný, D. 1999, *Icar*, **139**, 295
- Morbidelli, A., Tsiganis, K., Crida, A., Levison, H. F., & Gomes, R. 2007, *AJ*, **134**, 1790
- Morbidelli, A., Walsh, K. J., O'Brien, D. P., Minton, D. A., & Bottke, W. F. 2015, in *Asteroids IV*, ed. P. Michel et al. (Tucson, AZ: Univ. Arizona Press), 493
- Müller, T. G., & Blommaert, J. A. D. L. 2004, *A&A*, **418**, 347
- Murray, N. W., & Holman, M. J. 1997, *AJ*, **114**, 1246
- Nesvorný, D. 2011, *ApJL*, **742**, L22
- Nesvorný, D. 2015a, *AJ*, **150**, 68
- Nesvorný, D. 2015b, *AJ*, **150**, 73
- Nesvorný, D., & Ferraz-Mello, S. 1997, *Icar*, **130**, 247
- Nesvorný, D., Ferraz-Mello, S., Holman, M., & Morbidelli, A. 2002, in *Asteroids III*, ed. W. F. Bottke et al. (Tucson, AZ: Univ. Arizona Press), 379
- Nesvorný, D., Jenniskens, P., Levison, H. F., et al. 2010, *ApJ*, **713**, 816
- Nesvorný, D., & Morbidelli, A. 2012, *AJ*, **144**, 117
- Nesvorný, D., & Vokrouhlický, D. 2016, *ApJ*, **825**, 94
- Nesvorný, D., Vokrouhlický, D., & Deienno, R. 2014a, *ApJ*, **784**, 22
- Nesvorný, D., Vokrouhlický, D., Deienno, R., & Walsh, K. J. 2014b, *AJ*, **148**, 52
- Nesvorný, D., Vokrouhlický, D., & Morbidelli, A. 2007, *AJ*, **133**, 1962
- Nesvorný, D., Vokrouhlický, D., & Morbidelli, A. 2013, *ApJ*, **768**, 45
- Nicholson, P. D., Čuk, M., Sheppard, S. S., Nesvorný, D., & Johnson, T. V. 2008, in *The Solar System Beyond Neptune*, ed. M. A. Barucci et al. (Tucson, AZ: Univ. Arizona Press), 411
- Papaloizou, J. C. B. 2011, *CeMDA*, **111**, 83
- Papaloizou, J. C. B., & Larwood, J. D. 2000, *MNRAS*, **315**, 823
- Pierens, A., & Raymond, S. N. 2011, *A&A*, **533**, 131
- Roig, F., & Nesvorný, D. 2015, *AJ*, **150**, 186
- Singer, K. N., Schenk, P. M., Robbins, S. J., et al. 2015, in *AAS DPS Meeting*, **No. 47**, 102.02
- Thommes, E. W., Duncan, M. J., & Levison, H. F. 1999, *Natur*, **402**, 635
- Tsiganis, K., Gomes, R., Morbidelli, A., & Levison, H. F. 2005, *Natur*, **435**, 459
- Vernazza, P., Fulvio, D., Brunetto, R., et al. 2013, *Icar*, **225**, 517
- Vokrouhlický, D., Bottke, W. F., Chesley, S. R., Scheeres, D. J., & Statler, T. S. 2015, in *Asteroids IV*, ed. P. Michel et al. (Tucson, AZ: Univ. Arizona Press), 509
- Vokrouhlický, D., & Nesvorný, D. 2015, *ApJ*, **806**, 143
- Vokrouhlický, D., Nesvorný, D., Bottke, W. F., & Morbidelli, A. 2010, *AJ*, **139**, 2148
- Walsh, K. J., Morbidelli, A., Raymond, S. N., O'Brien, D. P., & Mandell, A. M. 2011, *Natur*, **475**, 206
- Weissman, P. R., Asphaug, E., & Lowry, S. C. 2004, in *Comets II*, ed. M. C. Festou et al. (Tucson, AZ: Univ. Arizona Press), 337